Inorg. Chem. **2008**, *47*, 5702−5719

Effect of Chelate Dynamics on Water Exchange Reactions of Paramagnetic Aminopolycarboxylate Complexes

Joachim Maigut, Roland Meier, Achim Zahl, and Rudi van Eldik*

Inorganic Chemistry, Department of Chemistry and Pharmacy, University of Erlangen-Nürnberg, Egerlandstrasse 1, 91058 Erlangen, Germany

Received December 19, 2007

Because of our interest in evaluating a possible relationship between complex dynamics and water exchange reactivity, we performed ^{1}H NMR studies on the paramagnetic aminopolycarboxylate complexes Fe^{II}−TMDTA and Fe^{II}−CyDTA and their diamagnetic analogues Zn^{II}−TMDTA and Zn^{II}−CyDTA. Whereas a fast $\Delta-\Lambda$ isomerization was observed for the TMDTA species, no acetate scrambling between in-plane and out-of-plane positions is accessible for any of the CyDTA complexes because the rigid ligand backbone prevents any configurational changes in the chelate system. In variable-temperature ^{1}H NMR studies, no evidence of spectral coalescence due to nitrogen inversion was found for any of the complexes in the available temperature range. The TMDTA complexes exhibit the known solution behavior of EDTA, whereas the CyDTA complexes adopt static solution structures. Comparing the exchange kinetics of flexible EDTA-type complexes and static CyDTA complexes appears to be a suitable method for evaluating the effect of ligand dynamics on the overall reactivity. In order to assess information concerning the rates and mechanism of water exchange, we performed variable-temperature and -pressure ^{17}O NMR studies of Ni^{II}−CyDTA, Fe^{II}−CyDTA, and Mn^{II}−CyDTA. For Ni^{II}−CyDTA, no significant effects on line widths or chemical shifts were apparent, indicating either the absence of any chemical exchange or the existence of a very small amount of the water-coordinated complex in solution. For $[Fe^{II}(CyDTA)(H_2O)]^{2-}$ and $[Mn^{II}(CyDTA)(H_2O)]^{2-}$, exchange rate constant values of $(1.1 \pm 0.3) \times 10^6$ and $(1.4 \pm 0.2) \times 10^8$ s^{-1}, respectively, at 298 K were determined from fits to resonance-shift and line-broadening data. A relationship between chelate dynamics and reactivity seems to be operative, since the CyDTA complexes exhibited significantly slower reactions than their EDTA counterparts. The variable-pressure ^{17}O NMR measurements for $[Mn^{II}(CyDTA)(H_2O)]^{2-}$ yielded an activation volume of $+9.4 \pm 0.9$ cm^3 mol^{-1}. The mechanism is reliably assigned as a dissociative interchange (I_d) mechanism with a pronounced dissociation of the leaving water molecule in the transition state. In the case of $[Fe^{II}(CyDTA)(H_2O)]^{2-}$, no suitable experimental conditions for variable-pressure measurements were accessible.

Introduction

Particular interest in investigations focusing on water exchange reactions of aminopolycarboxylate complexes in aqueous media arises from the fact that the reactivity of these complexes is controlled by the exchange kinetics of an additionally bound water ligand. The substitution of the water molecule is a desired reaction in, for example, NO scavenging processes in industrial and medical applications. On the other hand, the lability of the coordinated water molecule and the ease of its substitution enable unwanted side reactions in the presence of appropriate reactants, e.g., the reaction with oxygen. Thus, it was found that a functionalized (methidiumpropyl)Fe^{II}−EDTA complex efficiently cleaves DNA in the presence of molecular oxygen. The observed products were consistent with oxidative degradation of the deoxyribose ring of the DNA backbone, most probably via formation of hydroxyl radicals.[1] However, aminopolycarboxylate ligands are still necessary therapeutics, such as in chelation treatment of metal intoxication.[2] Furthermore, insufficient attempts to defeat childhood iron-deficiency anemia using flour fortified with iron powder led to new interest in the use of chelated iron for the treatment of

* To whom correspondence should be addressed. E-mail: vaneldik@chemie.uni-erlangen.de.

(1) Hertzberg, R. P.; Dervan, P. B. *Biochemistry* **1984**, *23*, 3934.
(2) Andersen, O. *Chem. Rev.* **1999**, *99*, 2683.

10.1021/ic702421z CCC: $40.75
Published on Web 05/30/2008

Scheme 1. Variations in the Ligand Backbone Linker and Their Impact on the Exocyclic Angle O_G-M-O_G (TMDTA) and the Feasibility of Ligand Rearrangements (CyDTA) of the Related Complexes

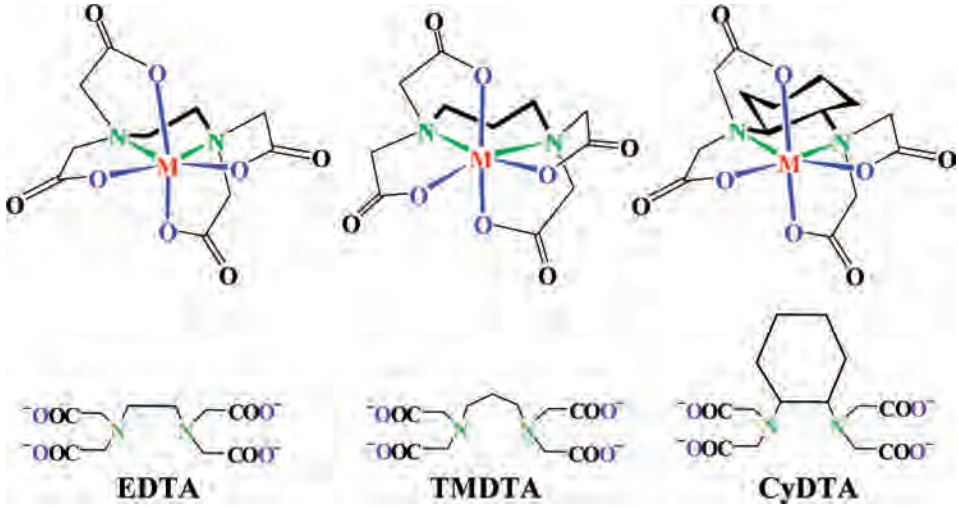

malnutrition. The intention was to overcome the poor bioavailability of nonchelated iron that primarily results from precipitation at the higher pH in the small intestine. Therefore, a Fe−EDTA complex, which is stable in the low pH medium of the stomach, was applied. High-dose EDTA-chelated iron supplements in cereals were required to beat childhood iron deficiency and reduced the prevalence of iron-deficiency anemia by 89%.[3]

In regard to the new interest in Fe−EDTA complexes as nutritional supplements for children, particularly with respect to the necessary concentrations, the enhanced reactivity of these compounds requires further clarification. Our earlier studies of the water exchange kinetics of Fe^{II}−EDTA revealed a rapidly exchanging water molecule, with a k_{ex} value of 2.7×10^6 s^{-1} at 298 K.[4] Systematic variations of the complex architectures can be attained by altering the ligand structures in a distinct way (see Scheme 1). It is our goal to explore the effects of these modifications on the kinetics and ligand exchange mechanisms in order to eventually understand appropriate interdependencies of the kinetic parameters and the solution structures on a higher level.

In the present work, the EDTA skeleton is varied in two ways (Scheme 1):

(i) The central diamine branch is elongated by one CH_2 group in going from EDTA to TMDTA.

(ii) The central diamine branch is made more rigid by the introduction of *trans*-cyclohexanediamine as the central diamine fragment in going from EDTA to CyDTA.

TMDTA complexes can be expected to exhibit fast ligand rearrangement similar to the EDTA species[4] but are known to extend their coordination numbers less readily than the corresponding EDTA complexes. Good examples illustrating this are the Ca^{2+} and Mg^{2+} complexes with EDTA and TMDTA. Whereas the larger Ca^{2+} ion is eight-coordinate in salts of $[Ca(EDTA)(H_2O)_2]^{2-}$,[5−7] it is only seven-coordinate in $[Ca(TMDTA)(H_2O)_2]^{2-}$.[8] In a similar way, the smaller Mg^{2+} ion is seven-coordinate in $[Mg(EDTA)(H_2O)]^{2-}$ salts[9,10] but six-coordinate in $[Mg(TMDTA)]^{2-}$.[8] One anticipates that these differences are related only to the simple elongation of the diamine branch in the ligand. CyDTA complexes are usually more stable (by 2−5 orders of magnitude) than their EDTA relatives.[11] Most of this increase is due to the greater preorganization of the donor groups of CyDTA over those of EDTA, which leads to a drastically increased ΔS contribution for formation of CyDTA complexes relative to that for EDTA complexes.[12]

In the present study, we used ^1H and ^{13}C NMR spectroscopy to investigate the consequences of the ligand variations shown in Scheme 1 on the solution structures of Fe^{II}−TMDTA and Fe^{II}−CyDTA as well as on their diamagnetic analogues Zn^{II}−TMDTA and Zn^{II}−CyDTA. We also studied the variation of the mechanistic details of the water exchange reactions in going from $[Fe^{II}(EDTA)(H_2O)]^{2-}$ to $[Fe^{II}(CyDTA)(H_2O)]^{2-}$ and from $[Mn^{II}(EDTA)(H_2O)]^{2-}$ to $[Mn^{II}(CyDTA)(H_2O)]^{2-}$. In previous contributions, we studied the solution structure and the mechanism of the water exchange reaction of $[Fe^{II}(EDTA)(H_2O)]^{2-}$ using NMR techniques.[4] In a subsequent comprehensive study, the relationships between the solution structures and water

(3) Andang'o, P. E. A.; Osendarp, S. J. M.; Ayah, R.; West, C. E.; Mwaniki, D. L.; De Wolf, C. A.; Kraaijenhagen, R.; Kok, F. J.; Verhoef, H. *Lancet* **2007**, *369*, 1799.
(4) Maigut, J.; Meier, R.; Zahl, A.; van Eldik, R. *Inorg. Chem.* **2007**, *46*, 5361.
(5) Barnett, B. L.; Uchtman, V. A. *Inorg. Chem.* **1979**, *18*, 2674.
(6) Arriortua, M. I.; Insausti, M.; Urtiaga, M. K.; Via, J.; Rojo, T. *Acta Crystallogr.* **1992**, *C48*, 779.
(7) Antsyshkina, A. S.; Sadikov, G. G.; Poznyak, A. L.; Sergienko, V. S. *Zh. Neorg. Khim.* **2002**, *47*, 43.
(8) Radanović, D. D.; Rychlewska, U.; Djuran, M. I.; Warżajtis, B.; Drasković, N. S.; Guresić, D. M. *Polyhedron* **2004**, *23*, 2183.
(9) Passer, E.; White, J. G.; Cheng, K. L. *Inorg. Chim. Acta* **1977**, *24*, 13.
(10) Stezowski, J. J.; Countryman, R.; Hoard, J. L. *Inorg. Chem.* **1973**, *12*, 1749.
(11) Hancock, R. D.; Martell, A. E. *Comments Inorg. Chem.* **1988**, *6*, 237.
(12) Martell, A. E.; Hancock, R. D. *Metal Complexes in Aqueous Solution*; Plenum Press: New York, 1997.

exchange mechanisms of the related pairs Ni^{II}−EDTA/Ni^{II}−TMDTA, Fe^{II}−EDTA/Fe^{II}−TMDTA, and Mn^{II}−EDTA/Mn^{II}−TMDTA were investigated.[13]

One major finding of this work is that all of the aminopolycarboxylate complexes studied so far {e.g., $[Fe^{II}(EDTA)(H_2O)]^{2-}$ [4] and $[Ni^{II}(EDTA)]^{2-}$ [13]} adopt fluxional rather than static solution structures. However, the extent to which the complex dynamics and the kinetics of solvent exchange are interrelated is still an unsettled question. The main tool used for such studies is NMR spectroscopy because it is a suitable method for both the detection of complex symmetry in solution and the analysis of the dynamics of the isomerization processes. Thus, new results on the interdependencies of the dynamic solution structures and the mechanisms of the solvent exchange reactions will be reported in the present study.

In a recent study of Gd^{III} chelates,[14] variations in the ligand backbone similar to those in the current work were found to influence the exchange rate of the inner-sphere water molecules in a significant way. The pyridine- and phosphonate-containing ligand was modified by introducing a cyclohexyl group into the ligand backbone, which led to a water exchange rate that was significantly slower than that of the ethylenediamine-brigded analogue.[14] Therefore, our study of transition-metal complexes with an analogous modification in the ligand (CyDTA vs EDTA) gives a complementary example of the impact of the properties of the coordination cage on the solution structure and the water exchange rates and mechanisms.

Experimental Section

Materials. All of the reagents used in this investigation were of analytical grade quality, and all of the solutions were prepared in doubly distilled water. Complexes of Zn^{2+} with the ligands H_4EDTA, H_4TMDTA, and H_4CyDTA (Acros Organics) were prepared as described elsewhere.[15] Fe^{II}−TMDTA and Fe^{II}−CyDTA were prepared by first dissolving 0.01 mol of H_4TMDTA and H_4CyDTA, respectively, in 10 mL of doubly distilled water. A clear solution was obtained after deprotonation with 2 equiv of K_2CO_3 followed by saturation with argon. $FeSO_4 \cdot 7H_2O$ (2.78 g) was added under strict exclusion of oxygen, and subsequent removal of the solvent gave the products as white precipitates that were isolated by filtration under nitrogen and dried under an oil-pump vacuum. For ^{1}H NMR spectroscopy, the solids so obtained were dissolved in D_2O. All of the spectra were successfully reproduced by intermediary-generated complexes. Here, the ligands were deprotonated by NaOD in D_2O solution and reacted directly with the iron salt under an argon atmosphere. In each case, the same spectrum and resonance pattern were obtained, with the disadvantage of a poor signal-to-noise ratio for the latter procedure. Each sample for the water exchange measurements was prepared by first dissolving the appropriate ligand in 0.1 M sodium acetate buffer solution (Fisher Chemical). The pH was measured using a Metrohm 713 pH meter with a Metrohm glass electrode (filled with NaCl instead of KCl to prevent precipitation of poorly soluble $KClO_4$) and adjusted to a value of 5.0 with NaOH (Acros Organics). The ionic strength was adjusted to $I = 0.5$ M using $NaClO_4$ (Merck). The solution was deoxygenated several times under vacuum and saturated with argon before the appropriate amount of $Ni(ClO_4)_2 \cdot 6H_2O$ (Fluka), $FeSO_4 \cdot 7H_2O$ (Acros Organics), or $Mn(ClO_4)_2 \cdot 6H_2O$ (Acros Organics) was added. The complex solution was enriched with ^{17}O by addition of argon-saturated $H_2{}^{17}O$ (10%, Deutero) using syringe techniques, giving a total ^{17}O enrichment of 1% in the measured samples.

^{1}H, ^{13}C, and ^{17}O NMR Measurements. The NMR spectra were recorded using a Bruker AVANCE DRX 400WB spectrometer equipped with a spectrospin superconducting widebore magnet (magnetic induction 9.4 T) at resonance frequencies of 400.14 MHz for ^{1}H, 100.61 MHz for ^{13}C, and 54.24 MHz for ^{17}O. The measurements on the Zn^{II}−EDTA, Zn^{II}−TMDTA, and Zn^{II}−CyDTA systems were performed in standard NMR tubes, whereas the oxygen-sensitive Fe^{II}−TMDTA and Fe^{II}−CyDTA samples were kept under an argon atmosphere in NMR tubes that were closed airtight by Teflon screw caps in order to avoid oxidative degradation during the measurements. The spectra were acquired in deuterium solvent-lock mode (D_2O) and referenced to 3-trimethylsilylpropionic acid [TSP, δ 0.0 (ppm)]. Two-dimensional ^{1}H−^{13}C HMQC correlation spectra of the zinc complexes were acquired in magnitude mode with decoupling during acquisition. Typical acquisition parameters for the diamagnetic complexes were the following: relaxation delay d1 = 1.5 s; 1/(2J)HX = 0.00345 s; a pulse length of 11 μs for ^{1}H (90°) with a power level of 0 dB, a sweep width of 4000 Hz, 4K data points, and 48 scans; and a pulse length of 7.4 μs for ^{13}C (90°) with a power level of −3 dB, a sweep width of 25 kHz, and 512 data points. Typical acquisition parameters for ^{1}H experiments on the paramagnetic complexes were a pulse length of 2.4 μs, a relaxation delay of 3.0 s, 248 scans, a sweep width of 100 kHz, and 65K data points.

Variable-temperature and -pressure data were referenced against aqueous buffer solutions, since line widths and shifts equal within experimental error to those obtained using Zn^{2+} complexes as diamagnetic references have been found (see also Balogh et al.[16]). Variable-temperature ^{17}O NMR measurements at atmospheric pressure were performed using a commercial 5 mm Bruker broadband probe thermostated with a Bruker B-VT 3000 variable-temperature unit. In the determination of the temperature-dependent shift of the ^{17}O resonance, the samples were sealed in glass spheres fitted inside a standard NMR tube in order to avoid susceptibility corrections of the measured data. The sample spheres were concentrically surrounded by an external deuterated standard (toluene) to ensure measurements in the deuterium-lock mode. Chemical shifts as well as line widths at half-height were determined using a deconvolution procedure on the real part of the Fourier-transformed spectra with a Lorentzian shape function in the data analysis module of Topspin. Variable-pressure measurements were performed using a homemade thermostated high-pressure probe,[17] where the sample was placed in a standard 5 mm NMR tube cut to a length of 50 mm and sealed by a moveable macor piston. The pressure was transmitted to the sample by pressurizing the surrounding perfluorated hydrocarbon (hexafluoropropylene oxide, Hostinert 175, Hoechst). The applied pressure in the probe was monitored using a VDO gauge with an accuracy of ±1%, and the temperature was adjusted to within ±0.1 K of the desired value using circulating, thermostatted water (Colora thermostat WK 16)

(13) Maigut, J.; Meier, R.; Zahl, A.; van Eldik, R. *J. Am. Chem. Soc.*, submitted for publication.
(14) Balogh, E.; Mato-Iglesias, M.; Platas-Iglesias, C.; Toth, E.; Djanashvili, K.; Peters, J. A.; de Blas, A.; Rodriguez-Blas, T. *Inorg. Chem.* **2006**, *45*, 8719.
(15) Li, F.; Song, R.; Liu, Q.; Mao, Y.; Qin, S. *Polyhedron* **1996**, *15*, 3829.
(16) Balogh, E.; He, Z.; Hsieh, W.; Liu, S.; Toth, E. *Inorg. Chem.* **2007**, *46*, 238.
(17) Zahl, A.; Neubrand, A.; Aygen, S.; van Eldik, R. *Rev. Sci. Instrum.* **1994**, *65*, 882.

Scheme 2. Schematic Representations of the Structures and Dynamics of the Diastereoisomers in the [M(EDTA)]/[M(EDTA)(H_2O)] System[a]

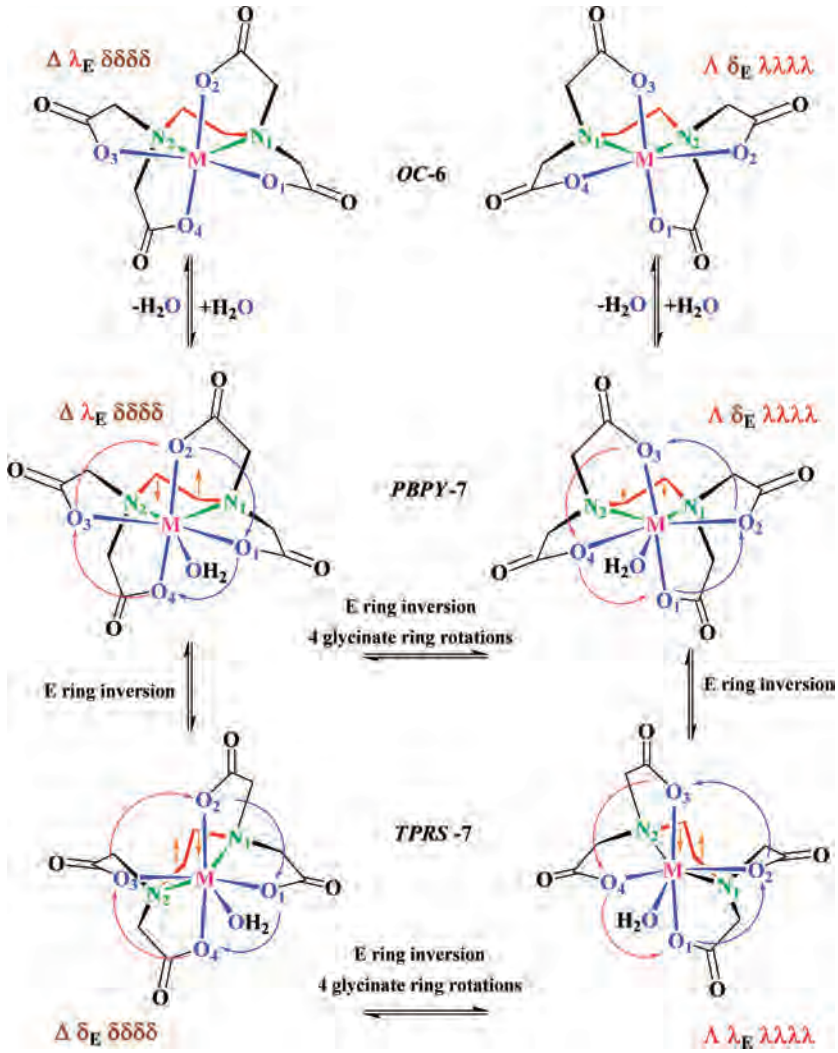

[a] The isomer denominations and chirality descriptors follow IUPAC rules,[37,38] and the abbreviations CTP and PB are used in the text for the *TPRS*-7 (capped trigonal prismatic) and *PBPY*-7 (pentagonal bipyramidal) seven-coordinate polytopes, respectively. The symbols Δ and Λ refer to the overall chiralities of the complexes, while λ and δ indicate the chiralities of individual chelate rings (the E subscript indicates the central diamine ring; no subscript is used for the remaining four glycinate rings). Horizontal pathways describe the Δ ⇌ Λ enantiomerizations Δ-PB ⇌ Λ-PB and Δ-CTP ⇌ Λ-CTP, which require one diamine ring inversion and four glycinate ring rotations, and vertical pathways show the diastereomer interconversion E,G/R ⇌ E,R/G[39] (where PB and CTP exhibit the E,G/R and E,R/G conformations, respectively[39]), which is realized by a single flip of the E ring. The details in this scheme reveal some similarities to Ln^{III}−DOTA m−M isomer equilibria (see Figures 1 and 2 in ref 40), where CTP resembles the m isomer and PB the M isomer.

and monitored before each measurement using an internal Pt-resistance thermometer having an accuracy of ±0.2 K.

Results and Discussion

Structural Features of Relevant EDTA, TMDTA, and CyDTA Complexes. 3d M^{III}−EDTA and −TMDTA Complexes. Combination of our previous results concerning mechanistic details of water exchange[4,13] with the stereochemical peculiarities of six- and seven-coordinate EDTA complexes[18–27] leads to the overall model for Δ−Λ isomerization shown in Scheme 2. The depictions in Scheme 2 reflect the rapid enantiomerizations that take place in aqueous solutions of EDTA complexes, where inversion of the central diamine ring [the E ring in EDTA and the T ring in TMDTA (see the right panels of Figures 1 and 2, respectively)] is accompanied by concerted rotations of the glycinate chelate rings during the Δ ⇌ Λ enantiomerization (see the horizontal pathways in Scheme 2). The application of the term "rotation" (introduced in this field during a study of the isomerizations of Ln^{III}−DOTA complexes[28]) is somewhat ambiguous in this context because two steps seem to occur:

(18) Gollogly, J. R.; Hawkins, C. J.; Wong, C. L. *Inorg. Nucl. Chem. Lett.* **1970**, *6*, 215.
(19) Gollogly, J. R.; Hawkins, C. J.; Beattie, J. K. *Inorg. Chem.* **1971**, *10*, 317.
(20) Pavelcik, F. *J. Coord. Chem.* **1984**, *13*, 299.
(21) Pavelcik, F.; Luptakova, E. *Collect. Czech. Chem. Commun.* **1990**, *55*, 1427.
(22) Hambley, T. W. *J. Comput. Chem.* **1987**, *8*, 651.
(23) Porai-Koshits, M. A.; Pozhidaev, A. I.; Polynova, T. N. *J. Struct. Chem.* **1974**, *15*, 1573.
(24) Dunitz, J. D. *Proc. Natl. Acad. Sci. U.S.A.* **1996**, *93*, 14260.
(25) Porai-Koshits, M. A. *Sov. Sci. Rev.* **1987**, *B10*, 91.
(26) Porai-Koshits, M. A.; Polynova, T. N. *Koord. Khim.* **1984**, *10*, 725.
(27) Meier, R. Habilitation Thesis, University of Leipzig, 2003.
(28) Hoeft, S.; Roth, K. *Chem. Ber.* **1993**, *126*, 869.

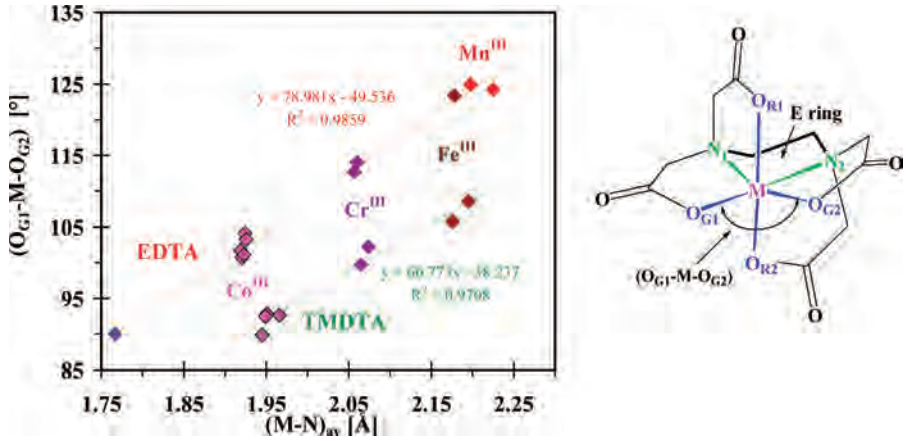

Figure 1. (left) Correlations of the sizes of the exocyclic angle $O_{G1}-M-O_{G2}$ with the average M−N distances $(M-N)_{av}$ in EDTA and TMDTA complexes containing six-coordinate 3d M^{III} ions. (right) Location of the exocyclic angle $O_{G1}-M-O_{G2}$ in a $[M(EDTA)]^-$ structure.

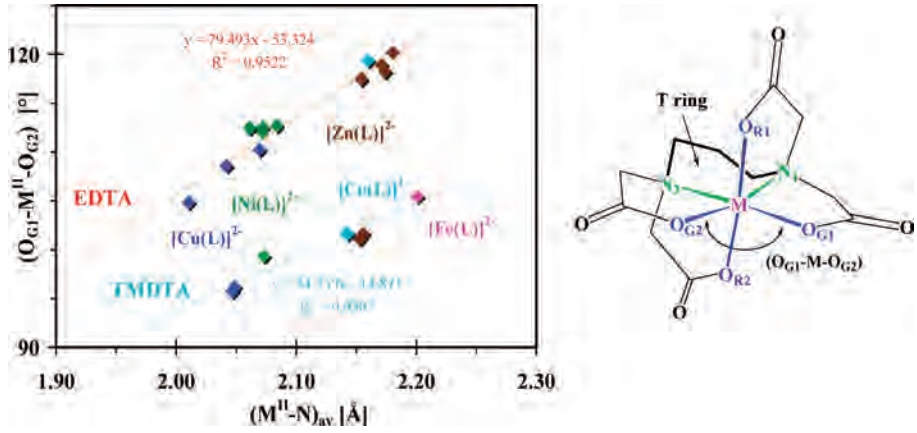

Figure 2. (left) Correlations between the average M−N distances $(M^{II}-N)_{av}$ and the $O_{G1}-M^{II}-O_{G2}$ angles for 3d M^{II}−EDTA and −TMDTA complexes (analogous to those in Figure 1). (right) Structure of the twist-boat form of a $[M(TMDTA)]^{2-}$ complex, showing the location of the $O_{G1}-M^{II}-O_{G2}$ angle.

a turn through space along a Berry-like pseudorotation pathway[29] (indicated by the half-circle arrows in Scheme 2) that is then coupled to the $\delta \rightleftharpoons \lambda$ rearrangements of the four glycinate rings. In reality, however, one can regard this rotation as a concerted step in which the glycinate rings change chirality by low-energy tunneling through a planar intermediate, as described in detail by Hawkins et al.[30,31] and others.[20,21,33,34] As outlined by Pavelcik,[20] the main part of this sort of rearrangement in the glycinate rings is realized by movement of the methylene carbon atom, which changes its state of hybridization continuously from sp^3 to sp^2 and vice versa. Experimental examples for structures representing the various species depicted in Scheme 2 include the initial increase in coordination number of the six- and seven-coordinate lithium salts of Fe^{III}−EDTA, namely, $Li[Fe(EDTA)]\cdot 3H_2O$[35] and $Li[Fe(EDTA)(H_2O)]\cdot 2H_2O$,[36] respectively.

Examples of seven-coordinate complexes of the type $[M(EDTA)(H_2O)]^-$ and $[M(EDTA)(H_2O)]^{2-}$ containing a central 3d transition-metal ion that can adopt both the pentagonal bipyramidal (PB) and capped trigonal prismatic (CTP) conformations include $[Ti(EDTA)(H_2O)]^-$,[41–43] $[Mn(EDTA)(H_2O)]^{2-}$,[44–48] and $[Fe(EDTA)(H_2O)]^{2-}$.[49,50] A study of the dependence of the structural features of $[Mn(EDTA)(H_2O)]^{2-}$ salts on the identity of the countercation has revealed that the interconversions between the seven-coordinate diastereomers shown in Scheme 2 can be mapped by the various salt

(29) Berry, R. S. *J. Chem. Phys.* **1960**, *32*, 933.
(30) Gollogly, J. R.; Hawkins, C. J.; Wong, C. L. *Inorg. Nucl. Chem. Lett.* **1970**, *6*, 215.
(31) Hawkins, C. J.; Palmer, J. A. *Coord. Chem. Rev.* **1982**, *44*, 1.
(32) Deleted in press.
(33) Juranic, N.; Niketic, S. R.; Andjelkovic, V.; Juranic, I. *J. Mol. Struct.* **1992**, *271*, 209.
(34) Harris, S. E.; Pascual, I.; Orpen, A. G. *J. Chem. Soc., Dalton Trans.* **2001**, 2996.
(35) Novozhilova, N. V.; Polynova, T. N.; Porai-Koshits, M. A.; Pechurova, N. I.; Martynenko, L. I.; Khadi, A. *Zh. Strukt. Khim.* **1973**, *14*, 745.
(36) Lind, M. D.; Hamor, M. J.; Hamor, T. A.; Hoard, J. L. *Inorg. Chem.* **1964**, *3*, 34.
(37) IUPAC. *Nomenklatur der Anorganischen Chemie*; VCH: Weinheim, Germany, 1995; pp 224−227.
(38) Jensen, K. A. *Inorg. Chem.* **1970**, *9*, 1.
(39) Porai-Koshits, M. A.; Pozhidaev, A. I.; Polynova, T. N. *Zh. Strukt. Khim.* **1974**, *15*, 1117.
(40) Aime, S.; Botta, M.; Fasano, M.; Marques, M. P. M.; Geraldes, C. F. G. C.; Pubanz, D.; Merbach, A. E. *Inorg. Chem.* **1997**, *36*, 2059.
(41) Mizuta, T.; Wang, J.; Miyoshi, K. *Inorg. Chim. Acta* **1993**, *203*, 249.
(42) Mizuta, T. Wang, J.; Miyoshi, K. *Bull. Chem. Soc. Jpn.* **1993**, *66*, 3662.
(43) Miyoshi, K.; Wang, J.; Mizuta, T. *Inorg. Chim. Acta* **1995**, *228*, 165.
(44) Richards, S.; Pedersen, B.; Silverton, J. V.; Hoard, J. L. *Inorg. Chem.* **1964**, *3*, 27.

structures.[51] Scheme 2 is needed in our work to understand the driving force for the fluxional-appearing ligand skeletons reflected in the NMR spectra of the Fe^{II}− and Zn^{II}−TMDTA and −EDTA complexes. There also seem to be driving forces that are responsible for the observation that EDTA complexes of metals can undergo the processes shown in Scheme 2 even though no seven-coordinate complexes were isolated in the solid state, for which we would like to offer a common explanation.

The exchange of solvent water at six-coordinate 3d M^{III} and M^{II} centers bound to hexadentate EDTA and TMDTA ligands seems to be stereochemically activated to a considerable extent. This effect is enhanced smoothly with increasing ionic radius. It has been pointed out that EDTA is too small to encircle even metal ions as small as Co^{III} (low-spin d^6, Shannon radius = 0.545 Å) in such a way that a regular octahedron can be formed.[52] This leads to a "hole" in the architecture of the EDTA complex opposite the central diamine ring (E ring), as has been described in a very detailed way.[52] This hole becomes larger as the ionic radius increases, because the hole size is a function of the ionic radius of the metal ion and thus of the M−N distance. The longer the average M−N distance $(M-N)_{av}$, the larger the exocyclic angle $O_{G1}-M-O_{G2}$ (a practical measure of the hole size) becomes. Figure 1 shows correlations of $(M-N)_{av}$ and $O_{G1}-M-O_{G2}$ for EDTA and TMDTA complexes of Co^{III}, Cr^{III}, Fe^{III}, and Mn^{III}. The correlation for EDTA reveals that achieving the ideal value of 90° for the $O_{G1}-M-O_{G2}$ angle in a six-coordinate EDTA complex would require a value of 1.767 Å for $(M-N)_{av}$, which is too small for any 3d ion.

It is therefore not surprising that the average size[53] of the exocyclic angles in the five $[Co(EDTA)]^-$ structures[53–56] compiled in Figure 1 ($(O_{G1}-M-O_{G2})_{av}$ = 102.2°) differs by 12.2° from the ideal value of 90° for a regular O_h structure. Previously, this relatively large hole seemed to be one of the reasons for the conclusion that the mechanism of racemization of $[Co(EDTA)]^-$ in alkaline solution proceeds via a seven-coordinate intermediate of the type $[Co(EDTA)(OH)]^{2-}$.[57] Because this process takes place only after extension of the coordination number, Basolo and Pearson[58] later extended this mechanistic picture to include racemization at neutral or weakly acidic pH, with the seven-coordinate species $[Co(EDTA)(H_2O)]^-$ as the intermediate.

The other EDTA-containing structures used in the compilation of Figure 1 included the lithium and potassium salts of the six-coordinate anion $[Cr(EDTA)]^-$, namely, $Li[Cr(EDTA)]\cdot 3H_2O$ and $K[Cr(EDTA)]\cdot 2H_2O$,[59] the six-coordinate form of the Fe^{III}−EDTA lithium salt $Li[Fe(EDTA)]\cdot 3H_2O$,[35] and two independent data sets for the structure of $K[Mn(EDTA)]\cdot 2H_2O$.[60,61] For the compilation of the $[M(TMDTA)]^-$ structures, four Co^{III} items were considered: $K[Co(TMDTA)]\cdot 2H_2O$[62] as well as three salts of $[Co(DPOT)]^-$ (DPOT = 2-hydroxy-1,3-propanediamine-*N*,*N*,*N*′,*N*′-tetraacetate).[63–65] The data used for $[Cr(TMDTA)]^-$ belonged to the structures of $Na[Cr(TMDTA)]\cdot 3H_2O$[66] and $Li[Cr(TMDTA)]\cdot 3H_2O$.[67] The $[Fe(TMDTA)]^-$ parameters were those found for the structures of the sodium $\{Na[Fe(TMDTA)]\cdot 3H_2O\}$[68] and guanidinium $(\{C(NH_2)_3\}[Fe(TMDTA)]\cdot 2H_2O)$[69] salts. The correlations in Figure 1 show very clearly that nucleophilic attack of the solvent (water) is facilitated with increasing effectiveness at metal centers in six-coordinate 3d M^{III}−EDTA and −TMDTA complexes as the value of $(M-N)_{av}$ increases. Since aqueous racemization of $[Co(EDTA)]^-$ (containing the small Co^{III} central ion) has been found to take place along a pathway as expressed by reaction 1, there seems to be no doubt that the related reaction for larger metal ions should proceed quite similarly.

$$[M^{III}(L)]^- + H_2O \overset{K_{6\rightarrow 7}}{\rightleftharpoons} [M^{III}(L)(H_2O)]^- \qquad (1)$$

In the case of $[Co(EDTA)]^-$ and $[Cr(EDTA)]^-$, no salts containing a seven-coordinate central ion with a coordinated water molecule could be isolated in the solid state. A special case is Fe^{III}−EDTA, where both $[Fe(EDTA)]^-$ and $[Fe(EDTA)(H_2O)]^-$ can be isolated as defined solids, in $Li[Fe(EDTA)]\cdot 3H_2O$[35] and $Li[Fe(EDTA)(H_2O)]\cdot 2H_2O$,[36] respectively. This does not mean that the equilibrium given in eq 1 is balanced in a way that allows measurable amounts of the species involved in the water exchange reaction to coexist in solution, because the value of the equilibrium

(45) Anan'eva, N. N.; Polynova, T. N.; Porai-Koshits, M. A. *Zh. Strukt. Khim.* **1974**, *15*, 261.
(46) Solans, X.; Gali, S.; Font-Altaba, M.; Oliva, J.; Herrera, J. *Afinidad* **1988**, *45*, 243.
(47) Yi, T.; Gao, S.; Li, B. *Polyhedron* **1998**, *17*, 2243.
(48) Polyakova, I. N.; Sergienko, V. S.; Poznyak, A. L. *Crystallogr. Rep.* **2002**, *47*, 245.
(49) Mizuta, T.; Wang, J.; Miyoshi, K. *Bull. Chem. Soc. Jpn.* **1993**, *66*, 2547.
(50) Mizuta, T.; Wang, J.; Miyoshi, K. *Inorg. Chim. Acta* **1995**, *230*, 119.
(51) Meier, R. Unpublished work.
(52) Weakliem, H. A.; Hoard, J. L. *J. Am. Chem. Soc.* **1959**, *81*, 549.
(53) Structures of the following salts of $[Co(EDTA)]^-$ were included in the correlation: $NH_4[Co(EDTA)]\cdot 2H_2O$ (ref 52), $[Co(NH_3)(sarp)]\cdot[Co(EDTA)]\cdot H_2O$ (ref 54), $[Co(en)_3][Co(EDTA)]_2Cl\cdot 10H_2O$ (ref 55), $[Mg(H_2O)_6][Co(EDTA)]\cdot 4H_2O$ (ref 56), and $[Ca(H_2O)_7][Co(EDTA)]_2$ (ref 56).
(54) Okamoto, K.-I.; Tsukihara, T.; Hidaka, J.; Shimura, Y. *Bull. Chem. Soc. Jpn.* **1978**, *51*, 3534.
(55) Warren, R. M. L.; Haller, K. J.; Tatehata, A.; Lappin, A. G. *Inorg. Chem.* **1994**, *33*, 227.
(56) Zasurskaya, L. A.; Pozdnyak, A. L.; Polynova, T. N.; Rybakov, V. B.; Porai-Koshits, M. A. *Zh. Neorg. Khim.* **1996**, *41*, 1647.
(57) Cooke, D. W.; Im, Y. A.; Busch, D. H. *Inorg. Chem.* **1962**, *1*, 13.
(58) Basolo, F.; Pearson, R. G. *Mechanisms of Inorganic Reactions*; Wiley: New York, 1967; Figure 4.25 on p 321 and accompanying text.
(59) Kushi, Y.; Morimasa, K.; Yoneda, H. *Abstracts of Papers*, 49th Annual Meeting of the Chemical Society of Japan, Tokyo, April, 1984; Abstract 1N31.
(60) Lis, T. *Acta Crystallogr.* **1978**, *B34*, 1342.
(61) Stein, J.; Fackler, J. P., Jr.; McClune, G. J.; Fee, J. A.; Chan, L. T. *Inorg. Chem.* **1979**, *18*, 3511.
(62) Nagao, R.; Marumo, F.; Saito, Y. *Acta Crystallogr.* **1972**, *B28*, 1852.
(63) Kalina, M.; Pavelcik, F.; Majer, J. *Collect. Czech. Chem. Commun.* **1978**, *43*, 3140.
(64) Sato, M.; Yano, S. *Bull. Chem. Soc. Jpn.* **1989**, *62*, 3932.
(65) Chen, X.-M.; Chen, H.-A.; Wu, B.-M.; Mak, T. C. *Acta Crystallogr.* **1996**, *C52*, 2693.
(66) Herak, R.; Srdanov, G.; Djuran, M. I.; Radanovic, D. J.; Bruvo, M. *Inorg. Chim. Acta* **1984**, *83*, 55.
(67) Meier, R. Unpublished work.
(68) Okamoto, K.; Kanamori, K.; Hidaka, J. *Acta Crystallogr.* **1990**, *C46*, 1640.
(69) Meier, R.; Maigut, J.; Kallies, B.; Lehnert, N.; Paulat, F.; Heinemann, F. W.; Zahn, G.; Feht, M. P.; Krautscheid, H.; van Eldik, R. *Chem. Commun.* **2007**, 3960.

constant $K_{6\rightleftharpoons7}$ is greater than 100 for the Fe^{III}−EDTA system at room temperature.[67]

Despite the fact that Li[Fe(EDTA)]·$3H_2O$ and Li[Cr(EDTA)]·$3H_2O$ are isostructural salts having virtually identical lattice constants, no water-containing phase of the Cr(III) complex can be crystallized from water as in the case for the Fe(III) analog. This feature is in line with the $K_{6\rightleftharpoons7}$ value of <0.01 for the Cr(III) species.[67] When one encounters equilibrium constants of this magnitude, application of temperature-dependent spectroscopy to elucidate the exact magnitude of the equilibrium constant is impossible. Therefore, in such systems it is most often not possible to specify the equilibrium constant for reaction 1 in an exact way. It is nevertheless quite obvious that a water concentration of 55.5 M and the "inviting" stereochemistry of EDTA and TMDTA complexes lead to equilibria of the reaction 1 type.

3d M^{II}−EDTA and −TMDTA Complexes. Correlations analogous to those shown in Figure 1 for 3d M^{III}−EDTA and −TMDTA complexes can also be made for appropriate 3d M^{II} complexes, as demonstrated in Figure 2.

The compilation of data in Figure 2 shows the structural interdependences of the average bond distances $(M^{II}-N)_{av}$ and exocyclic angles $O_{G1}-M^{II}-O_{G2}$ of 3d M^{II}−EDTA and −TMDTA complexes (similar to those shown in Figure 1 for the 3d M^{III}−EDTA and −TMDTA complexes). To correlate $(M^{II}-N)_{av}$ and $O_{G1}-M^{II}-O_{G2}$ for the $[M(EDTA)]^{2-}$ structures, data for the following salts were used: [{$Mn(H_2O)_4$}{Cu(EDTA)}]·$2H_2O$,[70] [{μ_2-Cu(en)$_2$}{Cu(EDTA)}$_2$][Cu(en)$_2$(H_2O)$_2$]·$4H_2O$,[71] and [{$Zn(H_2O)_4$}{Cu(EDTA)}]·$2H_2O$[72] for $[Cu(EDTA)]^{2-}$; [Cu(en)$_2$(H_2O)][Ni(EDTA)]·$3H_2O$,[73] Ca[Ni(EDTA)]·$4H_2O$,[74] [{$Ni(H_2O)_4$}{Ni(EDTA)}]·$2H_2O$,[75] and [Ni(en)$_3$][Ni(EDTA)]·$4H_2O$[76] for $[Ni(EDTA)]^{2-}$;[Mg(H_2O)$_4$][Zn(EDTA)]·$2H_2O$,[70][Cu(en)$_2$(H_2O)][Zn(EDTA)]·$3H_2O$,[77] and {$C(NH_2)_3$}$_3$[Zn(EDTA)]ClO_4·1.5H_2O[78] for $[Zn(EDTA)]^{2-}$; and [{$Co(H_2O)_4$}{Co(EDTA)}]·$2H_2O$[79] for $[Co(EDTA)]^{2-}$.

The correlation for the $[M(TMDTA)]^{2-}$ complexes was based on data for the following structures: [$Mn(H_2O)_6$][Cu(TMDTA)]·$2H_2O$[80] and [$Mg(H_2O)_6$][Cu(TMDTA)]·$2H_2O$[81] for Cu^{II}; [$Mg(H_2O)_6$][Ni(TMDTA)]·$2H_2O$[82] for Ni^{II}; [$Mg(H_2O)_6$][Co(TMDTA)]·$2H_2O$ and [$Co(H_2O)_6$][Co(TMDTA)]·$2H_2O$[83] for Co^{II}; and [$Mg(H_2O)_6$][Fe(TMDTA)]·$2H_2O$[84] for Fe^{II}.

A comparison of the slope and intercept of the regression line found for the 3d $[M(EDTA)]^-$ structures in Figure 1($y = 78.981x - 49.536$) with those for the $[M(EDTA)]^{2-}$ structures in Figure 2 ($y = 79.493x - 53.324$) reveals a close similarity, which leads to the logical conclusion that reaction 1′ is driven by the same forces as discussed for the M^{III}−EDTA systems, including increased opening of the $O_{G1}-M^{II}-O_{G2}$ angle with increasing $(M^{II}-N)_{av}$.

$$[M^{II}(L)]^{2-} + H_2O \overset{K_{6\rightleftharpoons7}}{\rightleftharpoons} [M^{II}(L)(H_2O)]^{2-} \qquad (1')$$

Figure 1 shows that the $O_{G1}-M-O_{G2}$ angles are considerably smaller in the TMDTA complexes than in their EDTA counterparts. While the average bond lengths $(M-N)_{av}$ are approximately identical for clusters of EDTA and TMDTA structures involving the same metal, the $O_{G1}-M-O_{G2}$ angles decrease in going from an EDTA to a TMDTA structure because encircling of the basal plane of the appropriate octahedron is much more effective in the latter than in the former. This is the main reason for a concurrent reduction in the magnitude of $K_{6\rightleftharpoons7}$ in going from EDTA to TMDTA complexes.

3d M^{III}− and M^{II}−CyDTA Complexes. Introduction of constraints into the ligand backbone can be regarded as suitable means of overcoming the fluxional behavior exhibited by labile EDTA-type complexes. Replacement of ethylenediamine by *trans*-1,2-cyclohexanediamine as the backbone linker has a number of significant stereochemical consequences, which are demonstrated in Scheme 3.

The stereochemical peculiarities of CyDTA complexes presented above allow some conclusions to be drawn concerning the solution structures of the three CyDTA complexes in the current study. In the case of Zn^{II}−CyDTA, two different structures have been found from crystal-structure analysis. In the case of [{$Zn(H_2O)_5$}{Zn(CyDTA)}]·H_2O,[85] the six-coordinate $[Zn(CyDTA)]^{2-}$ anion with an E,G/R conformation[86] was encountered. In [{$Zn(H_2O)_4$}{Zn(CyDTA)(H_2O)}]·$4H_2O$,[86] on the other hand, the ligand wraps around the Zn^{II} center to give the E,R/G conformation (see Figure S4 in the Supporting Information for details). As shown in Figure S4, the structure of $[Zn(CyDTA)(H_2O)]^{2-}$ can be regarded as pseudo-seven-coordinate because one of the in-plane O donor atoms is 3.135 Å away from the zinc center.

Sevenfold coordination in both $[Fe(CyDTA)(H_2O)]^{2-}$ and $[Mn(CyDTA)(H_2O)]^{2-}$ can be derived as follows. A seven-

(70) Solans, X.; Font-Altaba, M.; Oliva, J.; Herrera, J. *Acta Crystallogr.* **1983**, *C39*, 435.
(71) Sysoeva, T. F.; Agre, V. M.; Trunov, V. K.; Dyatlova, N. M.; Barkhanova, N. N. *Zh. Strukt. Khim.* **1984**, *25*, 107.
(72) Leonteva, M. V.; Fridman, A. Y.; Dyatlova, N. M.; Agre, V. M.; Sysoeva, T. F. *Zh. Neorg. Khim.* **1987**, *32*, 2494.
(73) Agre, V. M.; Sisoeva, T. F.; Trunov, V. K.; Fridman, A. Y.; Barkhanova, N. N. *Zh. Strukt. Khim.* **1981**, *22*, 114.
(74) Nesterova, Y. M.; Porai-Koshits, M. A. *Koord. Khim.* **1984**, *10*, 129.
(75) Coronado, E.; Drillon, M.; Fuertes, A.; Beltran, D.; Mosset, A.; Galy, J. *J. Am. Chem. Soc.* **1986**, *108*, 900.
(76) Sisoeva, T. F.; Agre, V. M.; Trunov, V. K.; Dyatlova, N. M.; Fridman, A. Y. *Zh. Strukt. Khim.* **1986**, *27*, 108.
(77) Sysoeva, T. F.; Starikova, Z. A.; Leonteva, M. V.; Dyatlova, N. M. *Zh. Strukt. Khim.* **1990**, *31*, 140.
(78) Meier, R. Unpublished work. This structure contains two crystallographically independent $[Zn(EDTA)]^{2-}$ ions in its asymmetric unit.
(79) McCandlish, E. F. K.; Michael, T. K; Neal, J. A.; Lingafelter, E. C.; Rose, N. J. *Inorg. Chem.* **1978**, *17*, 1383.
(80) Hernandez-Padilla, M.; Chinea, E.; Dominguez, S.; Mederos, A.; Munoz, M. C.; Lloret, F. *Polyhedron* **2000**, *19*, 1175.
(81) Rychlewska, U.; Radanovic, D. D.; Jevtovic, V. S.; Radanovic, D. J. *Polyhedron* **2000**, *19*, 1.
(82) Radanovic, D. J.; Ama, T.; Kawaguchi, H.; Draskovic, N. S.; Ristanovic, D. M.; Janicijevic, S. *Bull. Chem. Soc. Jpn.* **2001**, *74*, 701.
(83) Radanovic, D. D.; Rychlewska, U.; Djuran, M. I.; Draskovic, N. S.; Vasojevic, M. M.; Hodzic, I.M.; Radanovic, D. J. *Polyhedron* **2003**, *22*, 2745.
(84) Meier, R. Unpublished work.
(85) Polynova, T. N.; Filippova, T. V.; Porai-Koshits, M. A.; Bel'skii, V. K.; Sobolev, A. N.; Myachina, L. I. *Koord. Khim.* **1988**, *14*, 405.
(86) Fuertes, A.; Miravitlles, C.; Escriva, E.; Coronado, E.; Beltran, D.; Padel, L. J. *J. Chem. Soc., Dalton Trans.* **1989**, 863.

Scheme 3. Isomeric Equilibria of Six- And Seven-Coordinate CyDTA Complexes[a]

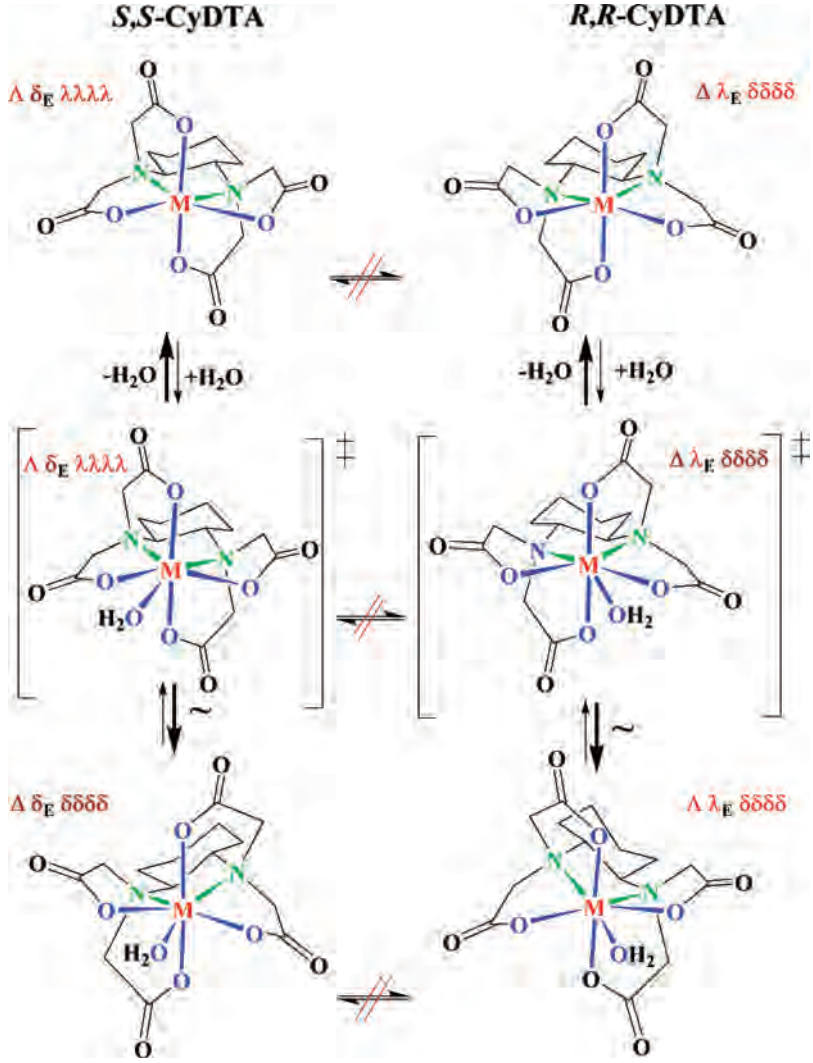

[a] Use of the commercial racemic ligand, which is a 50:50 mixture of (*S,S*)- and (*R,R*)-CyDTA, leads to the formation of the corresponding diastereomers, which are of the Λ δ_E type in the case of six-coordinate (*S,S*)-CyDTA complexes and the Δ λ_E type in the case of six-coordinate (*R,R*)-CyDTA complexes (the E,G/R form, according to Porai-Koshits et al.[23]). In contrast to the situation for the EDTA isomers shown in Scheme 2, the optical antipodes can no longer interconvert into each other because this would require bond breakage at the asymmetric carbon atoms. Thus, all of the horizontal pathways are frozen, and only interconversions along the vertical paths are possible. Simple water addition leads to the formation of the E,G/R form of the seven-coordinate PB complex. However, this species is unstable because of significant steric repulsion between R-ring protons (H_{11a} and H_{13b}) and axial protons (H_{3a} and H_{6a}) on the center carbons (C_3 and C_6, respectively) of the cyclohexane ring (the atom-labeling scheme and the $H_{11a}\cdots H_{6a}$ and $H_{13b}\cdots H_{3a}$ interactions are shown in Figures S5 and S6 in the Supporting Information). An explanation for the quasi-nonexistence of the seven-coordinate CyDTA PB species with the E,G/R conformation is given in the Supporting Information.

coordinate salt of the Mn^{II}−CyDTA complex[87] has been studied using X-ray diffraction, and the E,R/G (CTP) conformation was found in the solid state. Because the NMR data for $[Fe(CyDTA)(H_2O)]^{2-}$ revealed nonfluxional behavior in solution, both $[Fe^{II}(CyDTA)(H_2O)]^{2-}$ and $[Mn^{II}(CyDTA)(H_2O)]^{2-}$ should exist as seven-coordinate species in solution.

Solution Structure and Chelate Dynamics. In a previous paper, we reported the ^{1}H NMR spectra of $[Fe(EDTA)(H_2O)]^{2-}$.[4] The observed resonance pattern was successfully explained in terms of a dynamic averaging process, i.e., Δ−Λ isomerization. The interconversion between the mirror images having the Δ and Λ configurations occurs via scrambling of the two in-plane acetates into the out-of-plane position (and vice versa) with respect to the plane formed by the metal center and the two nitrogen donors. The methylene protons of the interchanging acetate groups remain nonequivalent throughout this process. One proton occupies an axial position and the other an equatorial position. In this respect, these methylene protons are labeled as axial out-of-plane (H_a^o), equatorial out-of-plane (H_e^o), axial in-plane (H_a^i), and equatorial in-plane (H_e^i). Consequently, if dynamic Δ−Λ interconversion occurs, this process leads to the proton exchanges $H_a^o \leftrightarrow H_e^i$ and $H_e^o \leftrightarrow H_a^i$. No acetate bond breakage is required for Δ ⇌ Λ interconversion, since this process can proceed by an entirely intramolecular twist-type mechanism (see Scheme 2) in which individual chelate rings change chirality via pseudorotational pathways. Such $\delta \rightleftharpoons \lambda$ flips of diamine chelate rings are called inversion

(87) Mosset, A.; Galy, J.; Munoz-Roca, C.; Real, J. A. *Z. Kristallogr.* **1990**, *193*, 21.

processes. However, the backbone configuration necessarily changes as a result of this acetate scrambling. Thus, this pathway for $\Delta-\Lambda$ interconversion is accessible for ligands whose backbones can undergo configurational changes. In this respect, EDTA has been shown to be a rather flexible ligand. However, to illustrate that this flexibility is a feature of not only EDTA but also EDTA-type ligands in general, we investigated complexes of the related TMDTA ligand, which differs from EDTA through elongation of the backbone by one methylene moiety. In contrast, ligand structures that prevent any configurational changes in the backbone, e.g., the rigid cyclohexane ring in CyDTA, lead to static solution structures for these complexes.

Before the paramagnetic complexes are discussed, the diamagnetic complexes will be considered. The principal spectral consequences of fast ligand rearrangement and static solution structure, respectively, are illustrated by the HMQC spectra of diamagnetic Zn^{II}−EDTA[88,89] and Zn^{II}−TMDTA[90] (representing flexible-backbone complexes) and Zn^{II}−CyDTA[88,91] (representing rigid-backbone complexes). The HMQC spectrum of Zn^{II}−EDTA is shown in Figure S1 in the Supporting Information. In Figure 3, the HMQC spectra of (A) Zn^{II}−TMDTA and (B) Zn^{II}−CyDTA are shown together. The F2 projection (top) is a conventional ^{1}H NMR spectrum, and the F1 projection (left) is a ^{13}C NMR spectrum; the obtained signals show directly coupled ^{1}H and ^{13}C nuclei.

The Zn^{II}−TMDTA complex, as a representative of the labile EDTA-type complexes, shows the aforementioned intramolecular rearrangement of the acetates between the in-plane and out-of-plane positions that leads to the proton exchanges $H_a^o \leftrightarrow H_e^i$ and $H_e^o \leftrightarrow H_a^i$. Therefore, the observed proton NMR spectrum consists of one AB resonance pattern (see the inset) with two doublets due to the geminal coupling of the diastereotopic methylene protons at 3.4096 and 3.1869 ppm (8H, $^2J = 16.7$ Hz) (also see the Zn^{II}−EDTA spectrum in Figure S1 in the Supporting Information). Variable-temperature studies revealed no spectral coalescence in the temperature range between the freezing and boiling points. Therefore, operation of a nitrogen inversion that exchanges the acetate groups belonging to the same nitrogen atom, i.e., $H_e^o \leftrightarrow H_e^i$ and $H_a^o \leftrightarrow H_a^i$, can be ruled out. The ^{13}C spectrum consists of an averaged ^{13}C signal at 64.45 ppm for the methylene carbon of the interchanging in-plane and out-of-plane acetate groups and a carboxylate resonance at 181.26 ppm.

The Zn^{II}−CyDTA complex shows the resonance pattern expected in the absence of any averaging process. Thus, as in other nonlabile systems such as Co^{III}−EDTA,[92] two sets of AB patterns for the methylene protons are observed, one due to geminal coupling of the methylene protons in out-of-plane positions (H_a^o and H_e^o) and the other assigned to the protons of the in-plane acetates. The assignment of the resonances is possible on the basis of a closer inspection of the geminal coupling constants (16.4 and 18.1 Hz, respectively), since the magnitude for ^2J coupling directly correlates with ring puckering.[93] It is known that five-membered rings in out-of-plane positions are less strained than those situated in-plane. In this respect, the larger absolute value for the coupling constant is observed for the out-of-plane glycinate protons at 3.32 and 3.43 ppm (4H, $^2J = 18.1$ Hz, $-CH_a^oH_e^o\,COO^-$), whereas the doublets at 2.88 and 3.72 ppm (4H, $^2J = 16.4$ Hz, $-CH_a^iH_e^i\,COO^-$) belong to the in-plane glycinate protons. The absence of acetate interchange leads to distinguishable ^{13}C signals for the in-plane (G-ring, 64.27 ppm) and out-of-plane (R-ring, 55.99 ppm) methylene carbons and the two carboxylate resonances at 181.26 and 181.91 ppm.

Severe line broadening for complexes with Fe^{3+} and Mn^{2+} prevented any NMR spectroscopic studies, whereas moderate line widths in the case of Fe^{2+} as the metal center enabled us to acquire information on the structures of the Fe^{II}−L complexes in aqueous solution. However, the investigations of paramagnetic Fe^{II}−TMDTA and Fe^{II}−CyDTA were complicated by contact- and pseudo-contact-shifted resonances, from which the diamagnetic contribution, which is directly correlated with structurally defined functional groups, was not easily accessible. The resonating nuclei in the vicinity of the metal center underwent substantial line broadening. Information from scalar couplings was missing since these couplings were entirely wiped out. However, assignments for paramagnetic substances could be obtained on the basis of signal integration and line widths, which allowed a tentative mapping of the distances of nuclei from the paramagnetic center.

The ^{1}H NMR spectra of Fe^{II}−TMDTA (Figure 4 and Figure S2 in the Supporting Information) in D_2O consist of four contact-shifted resonances, three shifted downfield and one upfield. The relative integrals allowed the assignment of the resonance at −77.70 ppm to the two protons of the β-CH_2 group in the ligand backbone. This assignment was supported by the observation of the line width ($\Delta\nu$) of 336.9 Hz, which is the smallest of the observed line widths, consistent with the spatial distance of the corresponding nuclei from the paramagnetic center. The remaining signals were equal in area, but the observed $\Delta\nu$ value of 367.5 Hz for the signal at 78.35 ppm allowed a reliable assignment to the four protons of the two α-CH_2 groups in the ligand backbone. The signals at 122.92 and 64.45 ppm refer to interchanging glycinate methylene protons $H_a^o \leftrightarrow H_e^i$ and $H_e^o \leftrightarrow H_a^i$, respectively. The solution behavior of Fe^{II}−TMDTA is dominated by fast $\Delta-\Lambda$ isomerization typical of flexible EDTA-type ligands. The chemical shifts and relative integrals are listed in Table 1 along with chemical shifts reported for Co^{II}−TMDTA.[94]

The ^{1}H NMR spectra of Fe^{II}−CyDTA (Figure 5) reveal a nonaveraged resonance pattern expected for systems in which acetate scrambling is impeded, e.g., Zn^{II}−CyDTA. It consists of four downfield-shifted and five upfield-shifted signals that

(88) Day, R. J.; Reilley, C. N. *Anal. Chem.* **1965**, *37*, 1326.
(89) Howarth, O. W.; Moore, P.; Winterton, N. *J. Chem. Soc., Dalton Trans.* **1974**, 2271.
(90) Farmer, M. J.; Howarth, O. W.; Moore, P. *J. Chem. Soc., Dalton Trans.* **1976**, 1445.
(91) Howarth, O. W.; Moore, P.; Winterton, N. *J. Chem. Soc., Dalton Trans.* **1975**, 360.
(92) Howarth, O. W. *Polyhedron* **1983**, *8*, 853.
(93) Jung, W.-S.; Chung, Y. K.; Shin, D. M.; Kim, S.-D. *Bull. Chem. Soc. Jpn.* **2002**, *75*, 1263.

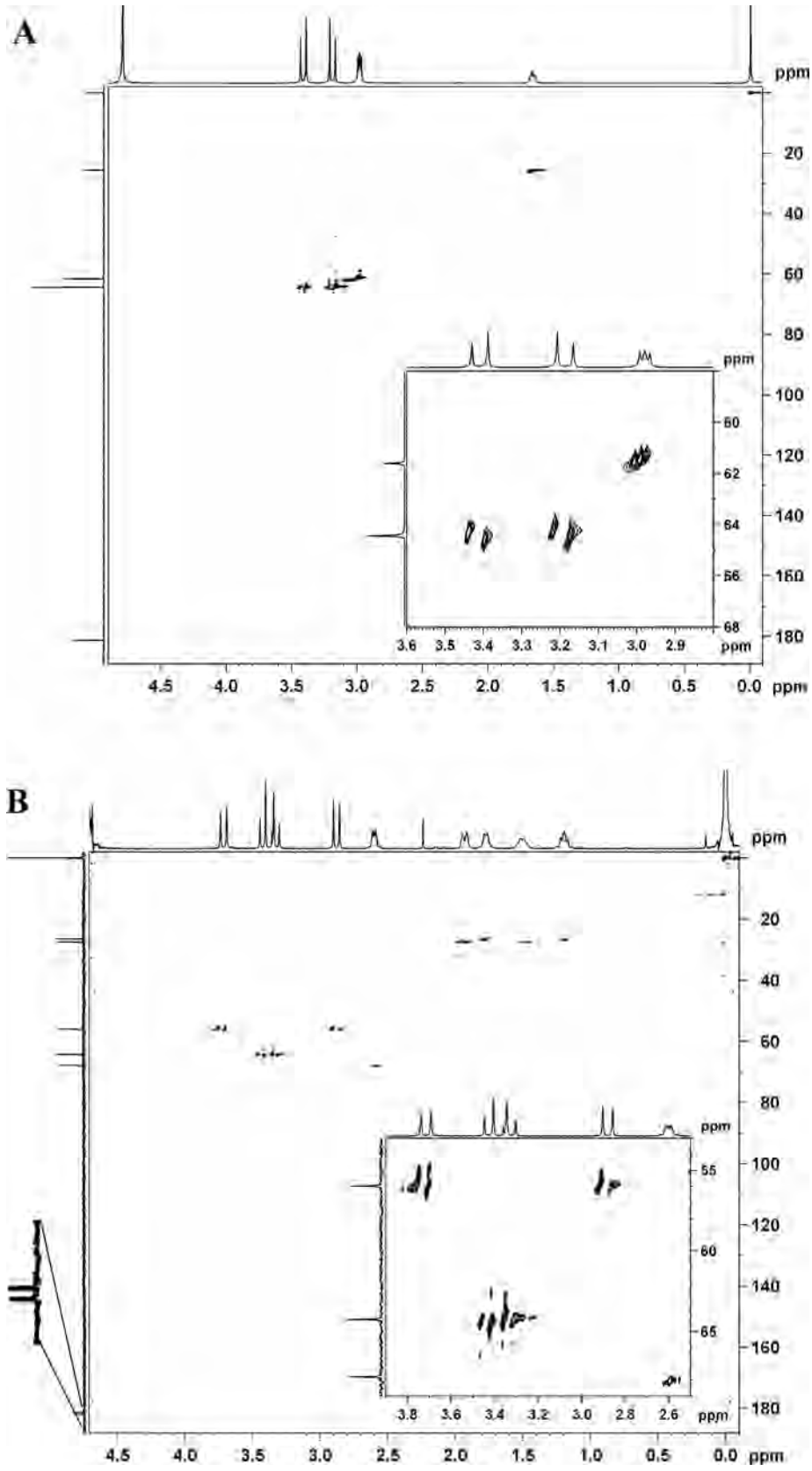

Figure 3. HMQC spectra of (A) Zn^{II}−TMDTA and (B) Zn^{II}−CyDTA. The insets show enlargements of the chemical shift ranges for the glycinate methylene protons. The resonance pattern in (A) reveals fast Δ−Λ interconversion in the TMDTA species. In contrast, the cyclohexyl ring in the backbone of the CyDTA complex prevents any acetate scrambling, as evidenced by the nonaveraged proton and carbon spectra obtained in (B): the enlarged carboxylate shift region shows two distinct signals that correspond to in-plane (G-ring) and out-of-plane (R-ring) carboxylates in the CyDTA complex.

are approximately equal in area (see Figure S3 in the Supporting Information). The relatively sharp peaks in the diamagnetic shift range at 10.30, −0.37, −6.16, and −14.22 ppm were assigned to cyclohexane ring protons (rp). The

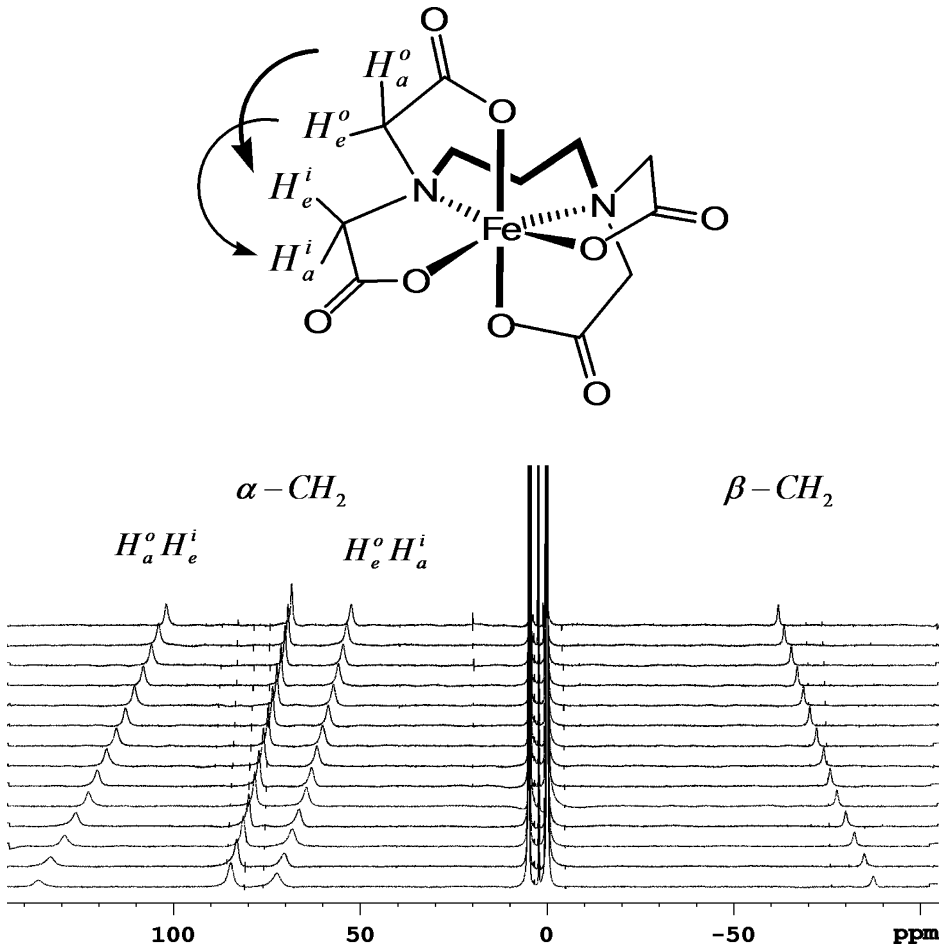

Figure 4. ^{1}H NMR spectra of paramagnetic, high-spin Fe^{II}−TMDTA in the temperature range from 278.2 K (lowermost spectrum) to 343.2 K (uppermost spectrum). The observed resonance patterns for the glycinate and backbone protons can be attributed to a dynamic Δ−Λ isomerization process (the water molecule has been omitted).

Table 1. Chemical Shifts (δ) and Corresponding Line Widths ($\Delta\nu$) for the Resonances of Fe^{II}−TMDTA, with Chemical Shifts for Co^{II}−TMDTA Also Listed for Comparison

Co^{II}−TMDTA[a]		Fe^{II}−TMDTA			
δ (ppm)	assignment	δ (ppm)	integral	$\Delta\nu$ (Hz)	assignment
110	$2H^o_a$, $2H^i_e$	122.92	4.07	704.1	$2H^o_a$, $2H^i_e$
55	2α-CH_2	78.35	4.25	367.5	2α-CH_2
33	$2H^o_e$, $2H^i_a$	64.45	4.00	654.1	$2H^o_e$, $2H^i_a$
−100	β-CH_2	−77.70	2.00	336.9	β-CH_2

[a] From ref 94.

resonance at 42.42 ppm was reliably assigned to the α-CH protons on the basis of the significant intermediate line width of 344.3 Hz, which is similar to that observed for the N-bound α-CH_2 moieties in the TMDTA complex. The remaining two downfield signals (at 81.28 and 56.53 ppm) and the two upfield signals (at −24.58 and −27.01 ppm) were assigned to the nonequivalent glycinate protons H^i_e, H^o_e, H^o_a, and H^i_a, respectively.

The temperature dependence of the contact shifts shows no deviations from linearity but large intercepts at zero inverse temperature. The observed paramagnetic chemical shifts (δ_{par}) obey the Curie law ($\delta_{par} = C/T$), since δ_{par} is inversely proportional to the absolute temperature T with unique Curie factors C for nonequivalent protons (Figure 6). From the variable-temperature contact-shift measurements, it can be concluded that a single species is present throughout the available temperature range. No evidence for detachment of an acetate group (curvature in the Curie plot) was found. In the available temperature range, the nitrogen inversion process is not an available pathway for Δ−Λ isomerization of the Fe^{II}−CyDTA complex, since any acetate-scrambling process can occur exclusively by lone-pair inversion of the nitrogen atoms. However, detachment of the nitrogen bonds in these systems usually has a higher activation energy because of the required M−N bond cleavage. The two factors responsible for a static solution structure are the hindered acetate rearrangement arising from the steric constraints of the cyclohexyl backbone and the higher activation energy necessary for nitrogen detachment, which impedes lone-pair inversion over the available temperature range. Since it can be assumed that nitrogen detachment is generally unfavorable for 3d transition-metal−CyDTA complexes at room temperature, one can expect that adoption of a static solution structure is not a feature of Fe^{II}−CyDTA exclusively but rather a general property of 3d transition-metal complexes with this type of ligand.

Our measurements show that the complex dynamics in solution is not exclusively controlled by properties of the metal center (as in inert Co^{III}−EDTA); ligand architecture, namely, constraints in the ligand backbone, can also

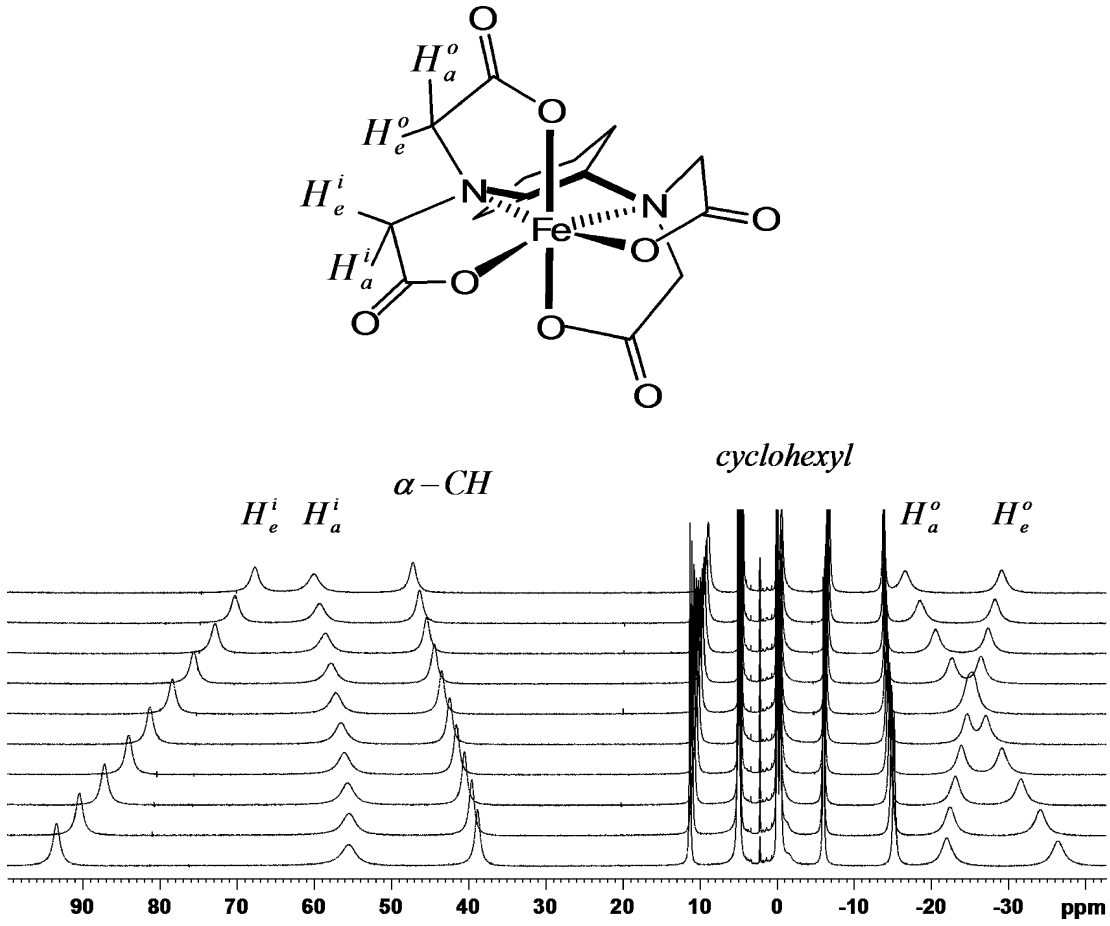

Figure 5. ^{1}H NMR spectra of paramagnetic, high-spin Fe^{II}−CyDTA in the temperature range from 278.2 K (lowermost spectrum) to 323.2 K (uppermost spectrum). The prevention of acetate scrambling by the rigid ligand backbone leads to distinct resonances for the protons of the in-plane and out-of-plane glycinate rings and for the backbone protons throughout the available temperature range.

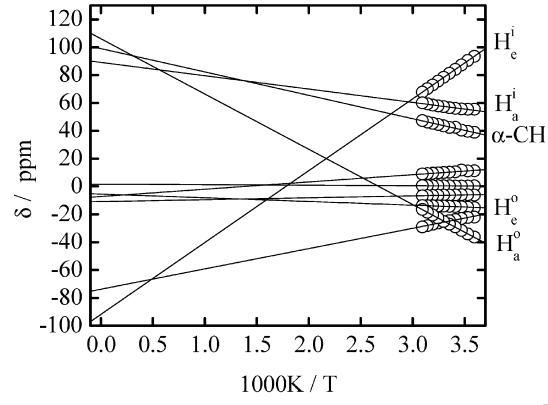

δ [ppm]	Δν [Hz]	assignment
81.28	428.7	H_e^i
56.53	660.4	H_a^i
42.42	344.3	α-CH
10.30	99.7	rp
-0.37	120.0	rp
-6.16	88.4	rp
-14.22	126.6	rp
-24.58	560.4	H_e^o
-27.01	624.2	H_a^o

Figure 6. (left) Curie plot for the experimental proton shifts of Fe^{II}−CyDTA. (right) Tabulated chemical shifts, line widths at 298.2 K, and signal assignments (rp = ring protons, α-CH = nitrogen-attached CH group with an axial orientation of the proton).

impede configurational changes for labile complexes. In contrast to the completely inert complexes (e.g., Co^{III}−EDTA), only ligand rearrangement is prevented, and exchange of additionally bound solvent molecules is still possible. The effect of this "frozen" solution dynamics on the reactivity of the complexes remains uncertain.

Water Exchange Reactions. Our particular interest in evaluating a possible relationship between complex dynamics and water exchange reactivity required additional kinetic studies using variable-temperature and -pressure ^{17}O NMR measurements. We applied the approach of Swift and Connick,[95,96] which connects the rates ($1/\tau_m$) for exchange

of solvent molecules between the bulk and the coordination site of a paramagnetic complex with the observable relaxation rates ($1/T_{2r}$) and resonance shifts ($\Delta\omega_r$) of the ^{17}O nuclei of bulk water molecules. Equation 2 illustrates the parameters that contribute to the transverse relaxation rate:

$$\frac{\pi}{P_m}(\Delta\nu_{obs} - \Delta\nu_{solvent}) = \frac{1}{T_{2r}} = \frac{1}{\tau_m}\left[\frac{{T_{2m}}^{-2} + (T_{2m}\tau_m)^{-1} + {\Delta\omega_m}^2}{({T_{2m}}^{-1} + {\tau_m}^{-1})^2 + {\Delta\omega_m}^2}\right] + \frac{1}{T_{2os}} \quad (2)$$

where $\Delta\nu_{obs}$ and $\Delta\nu_{solvent}$ are the full widths at half-height of the ^{17}O NMR signals of the bulk solvent in the presence and absence, respectively, of the paramagnetic compound, P_m is the mole fraction of bound water, T_{2m} represents the transverse relaxation time of coordinated water in absence of chemical exchange, $\Delta\omega_m$ is the difference in the resonance frequencies of bulk solvent and solvent in the first coordination sphere, τ_m is the mean lifetime of coordinated solvent, and T_{2os} is an outer-sphere contribution to T_{2r} that arises from long-range interactions of the paramagnetic unpaired electrons of the iron complex with water outside the inner coordination sphere. The first equality in eq 2 shows that $1/T_{2r}$ is related to difference in $\Delta\nu_{obs}$ and $\Delta\nu_{solvent}$ normalized to the mole fraction of bound water.

Equations 3a and 3b are obtained from simplification of eq 2 when contributions from T_{2os} and from both T_{2m} and T_{2os}, respectively, are negligible:

$$\frac{1}{T_{2r}} = \frac{1}{\tau_m}\left[\frac{{T_{2m}}^{-2} + (T_{2m}\tau_m)^{-1} + {\Delta\omega_m}^2}{({T_{2m}}^{-1} + {\tau_m}^{-1})^2 + {\Delta\omega_m}^2}\right] \quad (3a)$$

$$\frac{1}{T_{2r}} = \frac{1}{\tau_m}\left[\frac{{\Delta\omega_m}^2}{{\tau_m}^{-2} + {\Delta\omega_m}^2}\right] \quad (3b)$$

A modified form of eq 3b that relates $1/T_{2p}$ to the unnormalized difference in $\Delta\nu_{obs}$ and $\Delta\nu_{solvent}$ is given by eq 3c:

$$\pi(\Delta\nu_{obs} - \Delta\nu_{solvent}) = \frac{1}{T_{2p}} = \frac{P_m}{\tau_m}\left[\frac{{\Delta\omega_m}^2}{{\tau_m}^{-2} + {\Delta\omega_m}^2}\right] \quad (3c)$$

Equation 4, which relates the reduced chemical shift difference $\Delta\omega_r$ to T_{2m}, τ_m, and the chemical shift differences $\Delta\omega_m$ and $\Delta\omega_{os}$, is an additional source whereby kinetic data on solvent exchange can be extracted from an NMR observable, the chemical shift:

$$\Delta\omega_r = \frac{1}{P_m}(\omega_{obs} - \omega_0) = \frac{\Delta\omega_m}{(1 + \tau_m {T_{2m}}^{-1})^2 + {\tau_m}^2{\Delta\omega_m}^2} + \Delta\omega_{os} \quad (4)$$

The reduced chemical shift difference, $\Delta\omega_r$, was calculated as the difference in ω_{obs} and ω_0, the observed chemical shifts of the sample solution and the aqueous reference without the paramagnetic compound, respectively, normalized by the mole fraction of bound water. Whereas line-broadening experiments can be performed in standard NMR tubes, shift-analysis experiments require spherical NMR tubes in order to impede susceptibility effects on the chemical shift. In each experiment, the ^{17}O resonances were fitted with Lorentzian functions to give line widths and signal positions from the deconvolution.

Extraction of kinetic information from variable-temperature NMR measurements of transverse relaxation rate and reduced chemical shift difference requires consideration of the temperature dependence of the contributing parameters in eqs 2–4. For the temperature-dependent treatment of the bound water relaxation rate $1/T_{2m}$, an exponential Arrhenius-type temperature dependence (eq 5) was applied:

$$\frac{1}{T_{2m}} = \frac{1}{T_{2m}^0}\exp\left(\frac{E_m}{RT}\right) \quad (5)$$

where R is the gas constant. The dependence of the exchange rate constant (k_{ex}) on temperature was described by the Eyring equation (eq 6), which connects the reciprocal residence time $1/\tau_m$ ($=k_{ex}$) with the activation parameters (i.e., the activation enthalpy, $\Delta H^{\ddagger}$, and the activation entropy, $\Delta S^{\ddagger}$) for the water exchange process:

$$k_{ex} = \frac{1}{\tau_m} = \left(\frac{k_B T}{h}\right)\exp\left(\frac{\Delta S^{\ddagger}}{R} - \frac{\Delta H^{\ddagger}}{RT}\right) \quad (6)$$

where k_B is Boltzmann's constant and h is Planck's constant. For $\Delta\omega_m$, a reciprocal temperature dependence (eq 7) was applied, using the hyperfine coupling constant A/h as the proportionality constant that defines the relationship between the temperature variation and the chemical shift of the bound water molecule:

$$\Delta\omega_m = \frac{2\pi g_L \mu_B S(S+1)B}{3k_B T}\left(\frac{A}{h}\right) \quad (7)$$

The temperature dependence can be split into four principal ranges that have corresponding approximations (eqs 8–11) to the Swift−Connick equations:[97]

$$\text{Region I (very slow exchange):} \quad \frac{1}{T_{2r}} \approx \frac{1}{T_{2os}} \quad (8)$$

$$\text{Region II (slow exchange):} \quad \frac{1}{T_{2r}} \approx \frac{1}{\tau_m} \quad (9)$$

$$\text{Region III (fast exchange):} \quad \frac{1}{T_{2r}} \approx \tau_m{\Delta\omega_m}^2 \quad (10)$$

$$\text{Region IV (very fast exchange):} \quad \frac{1}{T_{2r}} \approx \frac{1}{T_{2m}} \quad (11)$$

Over the course of the temperature variation, the chemical shift difference, which is approximated by $\Delta\omega_r \approx \Delta\omega_{os}$ in the very slow exchange domain, shows a changeover to $\Delta\omega_r \approx \Delta\omega_m$ in the very fast exchange domain at higher temperatures. Inflection points in the plots of $\Delta\omega_r$ versus reciprocal temperature correspond to maxima in the relaxation plots.

The observed relaxation effects for $[Fe(CyDTA)(H_2O)]^{2-}$ with the most common complex concentration (20

(94) Everhart, D. S.; Evilia, R. F. *Inorg. Chem.* **1977**, *16*, 120.
(95) Swift, T. J.; Connick, R. E. *J. Chem. Phys.* **1962**, *37*, 307.
(96) Swift, T. J.; Connick, R. E. *J. Chem. Phys.* **1964**, *41*, 2553.
(97) Helm, L.; Nicolle, G.; Merbach, A. E. *Adv. Inorg. Chem.* **2005**, *57*, 327.

Table 2. Kinetic and NMR Parameters Derived from Variable-Temperature ^{17}O NMR Relaxation Measurements on $[Fe(CyDTA)(H_2O)]^{2-}$

parameter	fit results		
	fit A[a]	fit B[b]	fit C[c]
χ^2/DoF	0.00043	0.00033	0.00028
R^2	0.98337	0.98817	0.98858
A/h (Hz)[d]	1.0×10^7	1.0×10^7	1.0×10^7
$\Delta H^{\ddagger}$ (kJ mol^{-1})	15.7 ± 0.6	16.7 ± 0.9	17.7 ± 0.4
$\Delta S^{\ddagger}$ (J mol^{-1} K^{-1})	-74 ± 2	-72 ± 2	-70 ± 2
P_m	$(2.6 \pm 0.04) \times 10^{-4}$		
$K_{6\rightleftharpoons7}^{298}$	0.18	0.18 ± 0.02	0.21 ± 0.002
ΔH_r^0 (kJ mol^{-1})		-5.5 ± 2.9	-10^c
k_{ex} at 298.2 K (s^{-1})[e]	1.4×10^6	1.2×10^6	1.1×10^6

[a] Using a temperature-independent value of $K_{6\rightleftharpoons7}$. [b] Including the temperature dependence of $K_{6\rightleftharpoons7}$ using eqs 12 and 13. [c] Using a fixed value of -10 kJ mol^{-1} for ΔH_r^0 (see the discussion in the text). [d] A fixed value in all of the fits. [e] Calculated using eq 6 and the values of the activation parameters $\Delta H^{\ddagger}$ and $\Delta S^{\ddagger}$ obtained from the fits.

mM) were small, with $\Delta\nu_{obs} - \Delta\nu_{solvent} < 20$ Hz. However, at higher complex concentrations (100 mM), significant effects of temperature variation on ^{17}O relaxivities and chemical shifts were observed and provide clear evidence for the presence of an exchangeable inner-sphere water molecule (see Figure S7 in the Supporting Information). However, the assumption that the water-containing species $[Fe(CyDTA)(H_2O)]^{2-}$ is exclusively present in solution leads to a value for the hyperfine coupling constant significantly smaller than the one expected for a typical $Fe^{II}-O$ interaction. To account for the observation of an obviously smaller water-containing fraction, the $\ln(1/T_{2p})$ values obtained from the measured line widths were plotted against the reciprocal temperature. A fit of these data to eq 3c using a fixed A/h value of 1.0×10^7 Hz (the value for a typical $Fe^{II}-O$ interaction) and treating P_m as a free parameter yielded a P_m value of 2.6×10^{-4} (see Figure S8 in the Supporting Information and fit A in Table 2). On the basis of this result, we can safely conclude that only a minor portion of the total $[Fe^{II}-CyDTA]$ (100 mM) undergoes the water exchange process, with a mole fraction of 0.15.

The temperature dependence of reaction 1′ can be quantified using the temperature dependence of the equilibrium constant $K_{6\rightleftharpoons7}$ as expressed by eq 12:

$$K_{6\rightleftharpoons7}^{T} = K_{6\rightleftharpoons7}^{298} \exp\left[-\frac{\Delta H_r^0}{R}\left(\frac{1}{T} - \frac{1}{298.2\ \mathrm{K}}\right)\right] \qquad (12)$$

Consequently, an adequate description of the temperature-dependent variation of P_m is given by eq 13:

$$P_m = [\mathrm{complex}]\left[\frac{K_{6\rightleftharpoons7}^{T}}{(K_{6\rightleftharpoons7}^{T} + 1)}\right] \qquad (13)$$

A fit of the $\ln(1/T_{2p})$ data to eq 3c using eq 13 for P_m (Figure 7) yielded the parameters given as fit B in Table 2.

Comparison of the data obtained from fits A and B reveals that the activation parameters are rather insensitive to the effects of temperature on P_m. An interesting comparison can be made between the value of -5.5 ± 2.9 kJ mol^{-1} for ΔH_r^0 (the enthalpy of reaction 1′ with L = CyDTA) obtained from fit B (Table 2) and the ΔH_r^0 value of -10 kJ mol^{-1} found graphically as shown in Figure 8. This latter method of estimating the enthalpy of an equilibrium involving changes in coordination number caused by the addition or removal of a single water molecule is based on a description given by Hoard et al.[44] There the assumption is made that a plot of ΔH_r^0 for complex formation versus the atomic number of M^{II} (M = Mn, Fe, Co, Ni, Cu) should be virtually linear and strongly increasing throughout the series, so any "exothermic" deviation from this line can be regarded as an indication of the existence of seven-coordinate complexes of the type $[M(L)(H_2O)]$, where L is an open-chain hexadentate ligand. The data used to construct the diagram in Figure 8 were taken from the literature.[99] The value of ΔH_r^0 obtained in this way is the difference between the enthalpy of formation (ΔH_f) for seven-coordinate $[Fe^{II}(CyDTA)(H_2O)]^{2-}$ (eq 14a) and that for six-coordinate

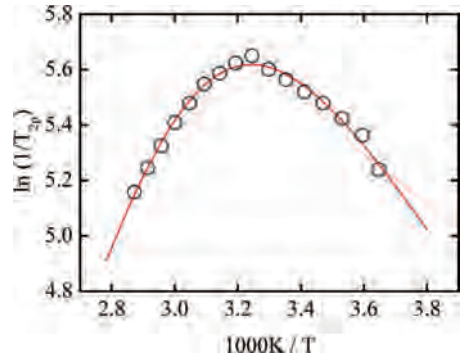

Figure 7. Plot of $\ln(1/T_{2p})$ data for $[Fe(CyDTA)H_2O]^{2-}$ (○) versus reciprocal temperature. The solid red line is a fit of the data to eq 3c using eq 13 for P_m (with eq 12 for $K_{6\rightleftharpoons7}^{T}$) to account for the temperature dependence of reaction 1′. The fit parameters are given as fit B in Table 2.

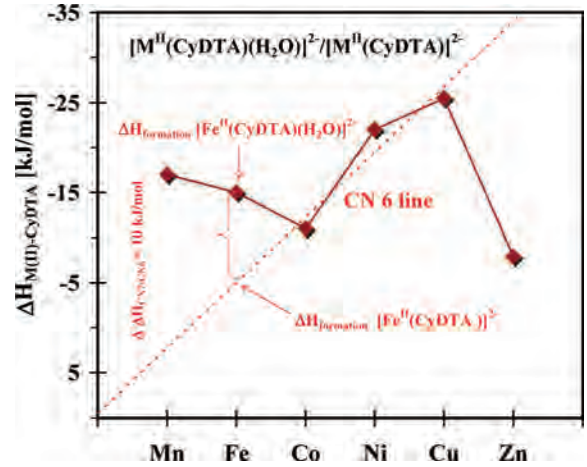

Figure 8. Plot of ΔH_f versus atomic number for $M^{II}-CyDTA$ (M = Mn, Fe, Co, Ni, Cu, Zn) complexes. The deviation of the value for $Fe^{II}-CyDTA$ from the virtually linear and strongly increasing correlation for the pure six-coordinate species throughout the series Mn, Fe, Co, Ni, and Cu (the "CN 6 line") is interpreted in terms of the formation of the water-containing seven-coordinate species $[Fe^{II}(CyDTA)(H_2O)]^{2-}$.[98,99]

(98) Deleted in press.

(99) (a) Wright, D. L.; Holloway, J. H.; Reilley, C. N. *Anal. Chem.* **1965**, *37*, 884. (b) Martell, A. E.; Smith, R. M.; Motekaitis, R. J. *NIST Critically Selected Stability Constants of Metal Complexes*, version 7; National Institute of Standards and Technology: Gaithersburg, MD, 2003.

Table 3. Rate and Activation Parameters for Water Exchange in M^{II}/M^{III}−CyDTA Complexes Derived from Variable-Temperature ^{17}O NMR Relaxation Experiments ($\Delta H^{\ddagger}$ and $\Delta S^{\ddagger}$) and the Pressure Dependence of the Exchange Rate Constant k_{ex} ($\Delta V^{\ddagger}$)

complex	k_{ex} at 298 K (s^{-1})	A/h (Hz)	$\Delta H^{\ddagger}$ (kJ mol^{-1})	$\Delta S^{\ddagger}$ (J K^{-1} mol^{-1})	$\Delta V^{\ddagger}$ (cm^3 mol^{-1})
$[Fe(CyDTA)(H_2O)]^{2-}$	$(1.1 \pm 0.3) \times 10^6$	1.0×10^7	17 ± 2	-71 ± 2	−
$[Fe(H_2O)_6]^{2+}$ [a]	$(4.4 \pm 0.3) \times 10^6$	9.4×10^6	41.4 ± 1.2	21 ± 5	3.8
$[Fe(CyDTA)(H_2O)]^{-}$ [b]	$(1.3 \pm 0.2) \times 10^7$	6.6×10^7 [c]	27.1 ± 1.0	-18 ± 4	4.0 ± 0.2
$[Mn(CyDTA)(H_2O)]^{2-}$	$(1.4 \pm 0.2) \times 10^8$	4.2×10^6	42.5 ± 0.8	54 ± 3	9.4 ± 0.9
$[Mn(H_2O)_6]^{2+}$ [a]	210×10^5	5.3×10^6	32.9 ± 1.3	5.7 ± 5.0	−5.4

[a] From ref 100. [b] From ref 101. [c] Calculated using the A value reported in ref 101.

$[Fe^{II}(CyDTA)]^{2-}$ (eq 14b), the latter of which is obtained from extrapolation of the "CN 6 line" as shown in Figure 8.[98]

$$[Fe^{II}(H_2O)_6]^{2+} + CyDTA^{4-} \overset{\log \beta^7_{110}}{\rightleftharpoons} [Fe^{II}(CyDTA)(H_2O)]^{2-} + 5H_2O \quad (14a)$$

$$[Fe^{II}(H_2O)_6]^{2+} + CyDTA^{4-} \overset{\log \beta^6_{110}}{\rightleftharpoons} [Fe^{II}(CyDTA)]^{2-} + 6H_2O \quad (14b)$$

The fixed ΔH^0_r value of −10 kJ mol^{-1} obtained from Figure 8, which we consider to be the limiting value for this parameter (see Figure S9 in the Supporting Information), was used to test the validity of the kinetic parameters via a third fit (fit C in Table 2). As before, the fit C results show that changing ΔH^0_r has only minor effects on the activation parameters. However, to account for the uncertainty in the activation parameters, we increased the error bars to include the data obtained from both fit B and fit C (Table 3).

Because of the relatively large T_{1e} values for Mn^{II} complexes, the T_{2m} contributions dominate in eq 3a and the contributions from $\Delta\omega_m$ are negligible, resulting in the simplified expression given by eq 3d:[102−105]

$$\frac{1}{T_{2r}} = \frac{1}{\tau_m + T_{2m}} \quad (3d)$$

In eq 3d, the transverse relaxation is dominated by the scalar relaxation mechanism $1/T_{2sc}$ given in eq 15:

$$\frac{1}{T_{2m}} \approx \frac{1}{T_{2sc}} = \frac{4\pi^2}{3} S(S+1)\left(\frac{A}{h}\right)^2 \tau_{s1} \quad (15)$$

where ω_s represents the Larmor frequency of the electron spin and τ_{s1} is given by

$$\frac{1}{\tau_{s1}} = \frac{1}{\tau_m} + \frac{1}{T_{1e}}$$

The longitudinal electronic relaxation term $1/T_{1e}$, which is the determining factor in transverse relaxation, is mainly governed by the transient zero-field splitting (ZFS) mechanism described by eq 16:[106]

$$\frac{1}{T_{1e}} = \frac{32}{25}\Delta^2\left(\frac{\tau_v}{1+\tau_v^2\omega_s^2} + \frac{4\tau_v}{1+4\tau_v^2\omega_s^2}\right) \quad (16)$$

in which Δ^2 is the trace of the square of the transient ZFS tensor and τ_v is the correlation time for modulation of the ZFS. Combining eqs 3d, 15, and 16 gives eq 3e, which provides an adequate description of the relevant contributions to T_{2r} for Mn^{II} species:

$$\frac{1}{T_{2r}} = \left[\tau_m + \frac{1}{C}\left(\frac{1}{\tau_m} + \frac{1}{T_{1e}}\right)\right]^{-1} \quad (3e)$$

where

$$C = \frac{4\pi^2}{3} S(S+1)\left(\frac{A}{h}\right)^2$$

Table 4. Kinetic and NMR Parameters Derived from Variable-Temperature ^{17}O NMR Relaxation Measurements on $[Mn(CyDTA)(H_2O)]^{2-}$

parameter	fit D[a]	fit E[b]
χ^2/DoF	0.00084	0.00067
R^2	0.99944	0.99955
C (s^{-2})	$(1.99 \pm 0.06) \times 10^{15}$	$(1.82 \pm 0.05) \times 10^{15}$
T_{1e} (s)	$(1.32 \pm 0.3) \times 10^{-7}$	1.55×10^{-7} [c]
$\Delta H^{\ddagger}$ (kJ mol^{-1})	42.9 ± 0.4	42.5 ± 0.4
$\Delta S^{\ddagger}$ (J mol^{-1} K^{-1})	54.8 ± 2	53.2 ± 2
τ_v^{298} (s)		1.8×10^{-12} [d]
Δ (rad s^{-1})		3.69×10^9 [d]
E_v (kJ mol^{-1})		11.6[e]

[a] Assuming a temperature-independent T_{1e} contribution. [b] Including the temperature dependence of T_{1e} by fitting the data with a temperature-dependent τ_v value. [c] Calculated from the parameters τ_v and Δ using eq 16. [d] Fixed values optimized using the values reported in ref 104. [e] Fixed value.

Because of the small contribution of T_{1e} to the overall relaxation time (see below), the data cannot define well all three of the parameters of T_{1e} (Δ, τ_v, and E_v) in a simultaneous fit. Thus, we first carried out a fit of the relaxation data to eq 3e assuming a temperature-independent T_{1e} contribution, as previously described in ref 102 (see fit D in Table 4 and Figure S10 in the Supporting Information). The T_{1e} value of 1.32×10^{-7} s obtained from fit D is close to the T_{1e} value of 1.27×10^{-7} s for $[Mn^{II}(EDTA)(H_2O)]^{2-}$ (from the parameters given in ref 104). Although the value of T_{1e} obtained from fit D already indicated a very minor contribution from the electronic relaxation, we attempted to account for a possible temperature dependence of T_{1e}, which required use of the parameters Δ and τ_v, with the temperature variation of τ_v expressed according to eq 17:

(100) Ducommun, Y.; Newman, K. E.; Merbach, A. E. *Inorg. Chem.* **1980**, *19*, 3696.
(101) Schneppensieper, T.; Seibig, S.; Zahl, A.; Tregloan, P.; van Eldik, R. *Inorg. Chem.* **2001**, *40*, 3670.
(102) Zetter, M. S.; Dodgen, H. W.; Hunt, J. P. *Biochemistry* **1973**, *12*, 778.
(103) Oakes, J.; Smith, E. G. *J. Chem. Soc., Faraday Trans. 1* **1983**, *79*, 543.
(104) Zetter, M. S.; Grant, M. W.; Wood, E. J.; Dodgen, H. W.; Hunt, J. P. *Inorg. Chem.* **1972**, *11*, 2701.
(105) Aime, S.; Anelli, L.; Botta, M.; Brocchetta, M.; Canton, S.; Fedeli, F.; Gianolio, E.; Terreno, E. *J. Biol. Inorg. Chem.* **2002**, *7*, 58.

$$\tau_v = \tau_v^{298} \exp\left[\frac{E_v}{R}\left(\frac{1}{T} - \frac{1}{298.2\ \mathrm{K}}\right)\right] \quad (17)$$

We applied the ESR parameters given for $[Mn^{II}(EDTA)(H_2O)]^{2-}$ in ref 100 as fixed starting values. The values of the parameters C, $\Delta H^{\ddagger}$, and $\Delta S^{\ddagger}$ so obtained were fixed, and Δ and τ_v were optimized with E_v adjusted to 11.6 kJ mol^{-1}.[104] These optimized values for Δ and τ_v (given in fit E in Table 4) yielded values of the kinetic parameters in excellent agreement with those obtained from the data treatment neglecting the temperature dependence of T_{1e}.

As a consequence, the aforementioned contribution from the electronic relaxation process to the overall relaxation is very small, i.e., $1/CT_{1e} \ll 1/C\tau_m$. The maximum contribution of the $1/CT_{1e}$ term is 6% at 283.2 K and less (3.5%) at the temperature of the high-pressure experiment (see Table S2-2). Figure 9 shows the experimental values of the transverse relaxation rate along with the three contributions to T_{2r} (see eq 3e) as functions of temperature. The kinetic parameters obtained for $[Mn(CyDTA)(H_2O)]^{2-}$ provide evidence for an exceedingly labile water molecule, with an exchange rate constant of $k_{ex} = (1.4 \pm 0.2) \times 10^8$ s^{-1} at 298 K (Table 3). This value of the exchange rate constant for $[Mn(CyDTA)(H_2O)]^{2-}$ is very close to the k_{ex} value of 1.32×10^8 s^{-1} measured for $[Mn(EDTA\text{-}BOM_2)(H_2O)]^{2-}$, where EDTA-$BOM_2$ is a side-chain-functionalized EDTA ligand.[105] Water substitution in the Mn^{II} chelate is 2 orders of magnitude faster than that in $[Fe(CyDTA)(H_2O)]^{2-}$, for which the calculated k_{ex} value is $(1.1 \pm 0.3) \times 10^6$ s^{-1} at 298 K (Table 3). The value of the hyperfine coupling constant for $[Mn(CyDTA)(H_2O)]^{2-}$, $A/h = 4.2 \times 10^6$ Hz, shows the value expected for an $Mn^{II}-O$ interaction. The considerably positive value of the activation entropy implies a dissociative character for the water exchange process.

However, to reliably identify the intimate exchange mechanism, variable-pressure measurements are required. These are best performed in the slow-exchange domain (region II), because of the direct proportionality between $1/T_{2r}$ and $k_{ex} = 1/\tau_m$ (eq 9), or in the fast-exchange domain (region III), if the chemical shift difference is large (eq 10). From the temperature dependence of the rate for $[Fe(CyDTA)(H_2O)]^{2-}$ (Figure 7), it is obvious that neither region II nor region III is fully accessible. For this reason, no suitable temperature for performing reliable variable-pressure measurements was available. For $[Mn(CyDTA)(H_2O)]^{2-}$ (Figure 9), the linear segment close to the maximum in the plot of $\ln(1/T_{2r})$ versus $1/T$ (in region III) is accessible, and the variable-pressure experiment was performed at a corresponding temperature (303.2 K). Figure 10 shows the linear increase in the transverse relaxation rate over the pressure range 2−150 MPa. The solid line in Figure 10 results from a fit of the data to eq 3e using the pressure (p) dependence of k_{ex} given by eq 18:

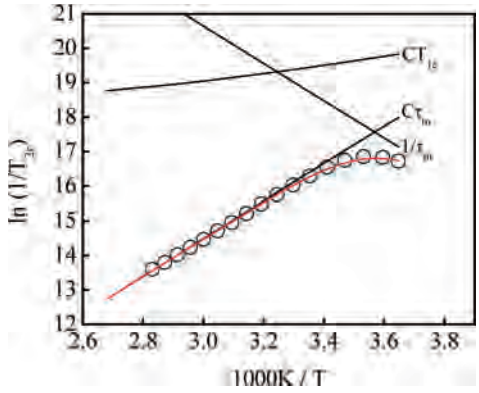

Figure 9. Temperature dependence of the reduced transverse relaxation rate for $[Mn(CyDTA)(H_2O)]^{2-}$ (○) and of the three contributions to T_{2r} (τ_m, $1/C\tau_m$, and $1/CT_{1e}$) specified in eq 3e (solid black lines). The solid red line is the least-squares fit to the data using eq 3e.

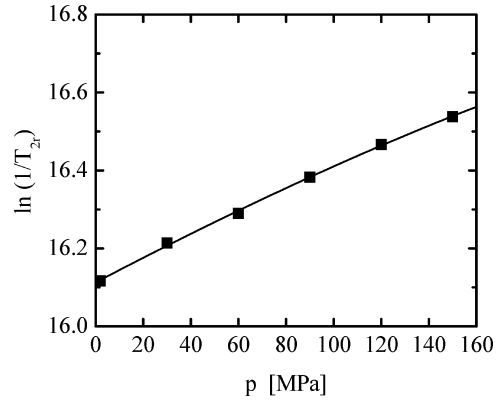

Figure 10. Pressure dependence of the reduced transverse ^{17}O relaxation rate for $[Mn(CyDTA)(H_2O)]^{2-}$ at 303.2 K (■). The solid line represents the least-squares fit of the data to eq 3e using eq 18 (see the text) with an activation volume of 9.4 ± 0.9 cm^3 mol^{-1}.

$$k_{ex} = \frac{1}{\tau_m} = (k_{ex})_0^T \exp\left(-\frac{\Delta V^{\ddagger}}{RT}p\right) \quad (18)$$

At this temperature, the contribution of the CT_{1e} term to T_{2r} is only 4.5%. Therefore, the effects of pressure on T_{1e} can safely be considered as negligible contributions to the observable transverse relaxation. In fact, ascribing to T_{1e} a pressure dependence having limiting values of +2 and −2 cm^3 mol^{-1} led to insignificant changes in the values of the free parameters $(k_{ex})_0^{303.2}$, $\Delta V^{\ddagger}$, and C (see Figure S11 in the Supporting Information). The parameter values $(k_{ex})_0^{303.2} = 1.79 \times 10^8$ s^{-1} and $C = 1.97 \times 10^{15}$ s^{-2} obtained from the variable-pressure data are in excellent agreement with those found in the variable-temperature experiment (1.83×10^8 s^{-1} and 1.99×10^{15} s^{-2}, respectively). On the basis of the reciprocal relation between $1/T_{2r}$ and k_{ex} resulting from the dominance of the overall relaxation by the $C\tau_m$ term at the applied temperature (see Figure 9), the faster relaxation is connected with a decrease in the water exchange rate. From this variation of the exchange rate constant with pressure at fixed temperature, the volume of activation ($\Delta V^{\ddagger}$), defined as the difference between the partial molar volumes of the transition and reactant states, can be obtained.[107–109]

The water exchange reaction was significantly slower at higher pressures. The value of 9.4 ± 0.9 cm^3 mol^{-1} determined for $\Delta V^{\ddagger}$ suggests that the exchange reaction proceeds via a dissociatively activated interchange (I_d)

(106) McLachlan, A. D. *Proc. R. Soc. London* **1964**, *A280*, 271.
(107) Whalley, E. *Adv. Phys. Org. Chem.* **1964**, *2*, 93.
(108) Eckert, C. A. *Annu. Rev. Phys. Chem.* **1972**, *23*, 239.
(109) Stranks, D. R. *Pure Appl. Chem.* **1974**, *38*, 303.

Table 5. Water Exchange Rate Constants (k_{ex}) at 298 K and Activation Volumes ($\Delta V^{\ddagger}$) for EDTA and CyDTA Complexes of Ni^{2+}, Fe^{2+}, Fe^{3+}, and Mn^{2+} and for the Corresponding Fully-Aquated Species

complex	k_{ex} (s^{-1})	$\Delta V^{\ddagger}$ ($cm^3\ mol^{-1}$)	source
$[Ni(H_2O)_6]^{2+}$	3.15×10^4	7.2	ref 100
$[Fe(H_2O)_6]^{2+}$	$(4.4 \pm 0.3) \times 10^6$	3.8	ref 100
$[Fe(H_2O)_6]^{3+}$	1.6×10^2	−5.4	refs 110 and 111
$[Mn(H_2O)_6]^{2+}$	2.1×10^7	−5.4	ref 100
$[Ni(EDTA')(H_2O)]^{2-}$	$(1.1 \pm 0.3) \times 10^6$	−	ref 13
$[Fe(EDTA)(H_2O)]^{2-}$	$(2.7 \pm 0.1) \times 10^6$	8.6 ± 0.4	ref 4
$[Fe(EDTA)(H_2O)]^{-}$	$(6.0 \pm 0.3) \times 10^7$	3.6 ± 0.1	ref 4
$[Mn(EDTA)(H_2O)]^{2-}$	$(3.2 \pm 0.1) \times 10^8$	3.0 ± 0.4	ref 13
$[Ni(CyDTA')(H_2O)]^{2-}$	−	−	this work
$[Fe(CyDTA)(H_2O)]^{2-}$	$(1.1 \pm 0.3) \times 10^6$	−	this work
$[Fe(CyDTA)(H_2O)]^{-}$	$(1.3 \pm 0.2) \times 10^7$	4.0 ± 0.2	ref 101
$[Mn(CyDTA)(H_2O)]^{2-}$	$(1.4 \pm 0.2) \times 10^8$	9.4 ± 0.9	this work

mechanism. Such a value for the activation volume is expected in the case of considerably shielded metal centers. Here, substitution of a water molecule requires significant dissociation of the leaving water molecule from the complex in the transition state in order to allow the entrance of a solvent molecule.

For Ni^{II}−CyDTA, no significant effects on line widths or chemical shifts were apparent, indicating either the absence of any chemical exchange or the existence of only a minor fraction of a water-containing species. Indeed, the formation of a seven-coordinate water-containing $[Ni^{II}(CyDTA)(H_2O)]^{2-}$ species seems virtually impossible in view of the size of the metal center. A six-coordinate structure similar to that of Ni^{II}−EDTA can be expected for a hexadentate chelator, with no tendency to depart from an octahedral structure.[112] A ring-opened species with a pentadentate chelate and a water molecule occupying the sixth coordination site, e.g., $[Ni^{II}(EDTA')(H_2O)]^{2-}$, is energetically disfavored because of steric constraints formed by the cyclohexyl ring in the ligand backbone. However, comparison of the available kinetic data (Table 5) for EDTA and CyDTA complexes reveals a clear trend. All of the studied CyDTA compounds show a significantly lower reactivity compared to their EDTA analogues.

Concluding Remarks

The lack of flexibility of the ligand backbone in the CyDTA complexes as opposed to their EDTA analogues seems to be the main reason for the decrease in k_{ex} values in going from the EDTA complexes to the corresponding CyDTA complexes (see Table 5). This rigidified metal coordination environment in the case of M−CyDTA complexes places significant constraints on the rearrangements required to reach the transition state, resulting in k_{ex}(CyDTA) < k_{ex}(EDTA) for all of the metal centers studied, with the largest impact observed for the higher-charged Fe^{III} chelate. For Mn^{II} and Fe^{II}, exchanging EDTA for CyDTA leads to decreases in reactivity by factors of 2, whereas in the case of Fe^{III}, water exchange is nearly 4.5 times slower for CyDTA than for EDTA complexes, which is comparable to the effect (4.7 times slower) found in the Gd^{III} study.[14] Although mechanistic data are not accessible for all of the complexes, the available activation volumes (Table 5) point to the necessity of a generally more pronounced dissociative character of the exchange mechanism for the CyDTA complexes than for the EDTA analogues. This is a necessary mechanistic consequence for water exchange in complexes having rigid spectator ligands, which hinder rearrangements on the way to the transition states for interchange processes.

In addition to the individual stereochemical influence of the chelate ligand on the exchange kinetics, water substitution for a given ligand motif depends largely on the properties of the metal center. Here, two factors that contribute significantly to the exchange kinetics in 3d transition metal complexes can be distinguished, namely, the charge density and the electronic configuration. The exchange kinetics for the trivalent iron species shows an acceleration of 5 orders of magnitude in the water exchange rate constant in going from the fully aquated complex to the EDTA complex. This can be interpreted in terms of a reduced effective charge on the metal center due to the σ-donating properties of the four acetate donor functionalities of the chelates. The observed k_{ex} values for the complexes of di- and trivalent metals with EDTA or CyDTA are found to be much closer than expected on the basis of the values for the fully aquated complexes. Here, partial cancellation of the effective charge on the metal center by the stronger donor groups of the chelate is operative and leads to the observation that the charge on the metal center plays a much smaller role in the exchange kinetics of aminopolycarboxylate complexes than in that of complexes with poor donor ligands such as water. For a given ligand motif (L = EDTA, CyDTA) the d-electron configuration remains the dominating criterion, and k_{ex} increases along the series Ni^{II}−L < Fe^{II}−L< Fe^{III}−L< Mn^{II}−L.

EDTA and TMDTA complexes of Fe^{II} and Zn^{II} show dynamic interconversions of the glycinate chelate rings ("arm rotation") in aqueous media, giving rise to Δ−Λ isomerization as the overall process. Introduction of steric constraints into the backbone of the aminopolycarboxylate ligand leads to suppression of the arm rotations in Zn^{II}/Fe^{II}−CyDTA, yielding a static solution structure. Decreases in the water exchange rates (and thus decreased reactivities) are observed for the CyDTA complexes of Fe^{II}, Fe^{III}, and Mn^{II} as compared with their EDTA counterparts. The relaxation data measured for Ni^{II}−CyDTA indicates either the absence of

(110) Grant, M. W.; Jordan, R. B. *Inorg. Chem.* **1981**, *20*, 55.
(111) Swaddle, T. W.; Merbach, A. E. *Inorg. Chem.* **1981**, *20*, 4212.
(112) Yamamoto, T.; Mikata, K.; Miyoshi, K.; Yoneda, H. *Inorg. Chim. Acta* **1988**, *150*, 231.

solvent exchange at the metal center or exchange in only an extremely small fraction of the water-containing species. The observed activation volumes show a pronounced dissociatively activated interchange mechanism. The presence of significant constraints on the rearrangements required to reach the transition state in the case of a rigid coordination cage seems to be the primary reason for the decreased reactivities of the CyDTA species as compared with their EDTA analogues and results in a more pronounced dissociative character for the water exchange reaction in the CyDTA complexes.

Acknowledgment. The authors gratefully acknowledge financial support from the Deutsche Forschungsgemeinschaft through SFB 583 on "Redox-Active Metal Complexes". R.M. is grateful to the Deutsche Forschungsgemeinschaft for support within the framework of Project ME 1148/7-1.

Supporting Information Available: HMQC spectra of Zn^{II}−EDTA (Figure S1); integrated ^{1}H NMR spectra of paramagnetic Fe^{II}−TMDTA (Figure S2) and Fe^{II}−CyDTA (Figure S3) as representative examples of complexes with fast ligand rearrangement and static solution structures, respectively; available structures of Zn^{II}−CyDTA complexes (Figure S4); an extended discussion of the structure of CyDTA complexes (Figures S5 and S6); and data and fits for the ^{17}O NMR relaxation measurements for $[Fe^{II}(CyDTA)(H_2O)]^{2-}$ (Table S1 and Figures S7−S9) and $[Mn^{II}(CyDTA)(H_2O)]^{2-}$ (Tables S2-1−S2-3 and Figures S10 and S11). This material is available free of charge via the Internet at http://pubs.acs.org.

IC702421Z